SN 2009ip à la PESSTO: no evidence for core collapse yet[*]

Morgan Fraser,[1][†] Cosimo Inserra,[1] Anders Jerkstrand,[1] Rubina Kotak,[1]
Giuliano Pignata,[2] Stefano Benetti,[3] Maria-Teresa Botticella,[4] Filomena Bufano,[2]
Michael Childress,[5] Seppo Mattila,[6] Andrea Pastorello,[3] Stephen J. Smartt,[1]
Massimo Turatto,[3] Fang Yuan,[5] Joe P. Anderson,[7] Daniel D. R. Bayliss,[5]
Franz Erik Bauer,[8,9] Ting-Wan Chen,[1] Francisco Förster Burón,[7] Avishay Gal-Yam,[10]
Joshua B. Haislip,[11] Cristina Knapic,[12] Laurent Le Guillou,[13] Sebastián Marchi,[7]
Paolo Mazzali,[3,14,15] Marco Molinaro,[12] Justin P. Moore,[11] Daniel Reichart,[11]
Riccardo Smareglia,[12] Ken W. Smith,[1] Assaf Sternberg,[14] Mark Sullivan,[16]
Katalin Takáts,[2] Brad E. Tucker,[5] Stefano Valenti,[17,18] Ofer Yaron,[10]
David R. Young[1] and George Zhou[5]

[1]*Astrophysics Research Centre, School of Mathematics and Physics, Queen's University Belfast, Belfast BT7 1NN, UK*
[2]*Departamento de Ciencias Fisicas, Universidad Andres Bello, Avda. Republica 252, Santiago, Chile*
[3]*INAF – Osservatorio Astronomico di Padova, Vicolo dell'Osservatorio 5, I-35122 Padova, Italy*
[4]*INAF – Osservatorio Astronomico di Capodimonte, Salita Moiariello 16, I-80131 Napoli, Italy*
[5]*Research School of Astronomy and Astrophysics, The Australian National University, Weston Creek, ACT 2611, Australia*
[6]*Finnish Centre for Astronomy with ESO (FINCA), University of Turku, Väisäläntie 20, FI-21500 Piikkiö, Finland*
[7]*Departamento de Astronomía, Universidad de Chile, Casilla 36-D, Santiago, Chile*
[8]*Pontificia Universidad Católica de Chile, Departamento de Astronomía y Astrofísica, Casilla 306, Santiago 22, Chile*
[9]*Space Science Institute, 4750 Walnut Street, Suite 205, Boulder, CO 80301, USA*
[10]*Benoziyo Center for Astrophysics, Weizmann Institute of Science, 76100 Rehovot, Israel*
[11]*University of North Carolina at Chapel Hill, Campus Box 3255, Chapel Hill, NC 27599-3255, USA*
[12]*INAF – Osservatorio Astronomico di Trieste, Via G.B. Tiepolo 11, I-34143 Trieste, Italy*
[13]*UPMC Univ. Paris 06, UMR 7585, Laboratoire de Physique Nucléaire et des Hautes Energies (LPNHE), F-75005 Paris, France*
[14]*Max-Planck-Institut für Astrophysik, Karl-Schwarzschildstr. 1, D-85748 Garching, Germany*
[15]*Astrophysics Research Institute, Liverpool John Moores University, Liverpool CH41 1LD, UK*
[16]*School of Physics and Astronomy, University of Southampton, Southampton SO17 1BJ, UK*
[17]*Las Cumbres Observatory Global Telescope Network, 6740 Cortona Dr, Suite 102, Goleta, CA 93117, USA*
[18]*Department of Physics, University of California, Santa Barbara, Broida Hall, Mail Code 9530, Santa Barbara, CA 93106-9530, USA*

ABSTRACT

We present ultraviolet, optical and near-infrared observations of the interacting transient SN 2009ip, covering the period from the start of the outburst in 2012 October until the end of the 2012 observing season. The transient reached a peak magnitude of $M_V = -17.7$ mag, with a total integrated luminosity of 1.9×10^{49} erg over the period of 2012 August–December. The light curve fades rapidly, dropping by 4.5 mag from the V-band peak in 100 d. The optical and near-infrared spectra are dominated by narrow emission lines with broad electron scattering wings, signalling a dense circumstellar environment, together with multiple components of broad emission and absorption in H and He at velocities in the range 0.5–1.2×10^4 km s^{-1}. We see no evidence for nucleosynthesized material in SN 2009ip, even in late-time pseudo-nebular spectra. We set a limit of <0.02 M$_\odot$ on the mass of any possible synthesized ^{56}Ni from the late-time light curve. A simple model for the narrow Balmer lines is presented and used to derive number densities for the circumstellar medium in the range $\sim 10^9$–10^{10} cm^{-3}. Our

near-infrared data do not show any excess at longer wavelengths, and we see no other signs of dust formation. Our last data, taken in 2012 December, show that SN 2009ip has spectroscopically evolved to something quite similar to its appearance in late 2009, albeit with higher velocities. It is possible that neither of the eruptive and high-luminosity events of SN 2009ip were induced by a core collapse. We show that the peak and total integrated luminosity can be due to the efficient conversion of kinetic energy from colliding ejecta, and that around 0.05–0.1 $M_\odot$ of material moving at 0.5–1×10^4 km s^{-1} could comfortably produce the observed luminosity. We discuss the possibility that these shells were ejected by the pulsational pair instability mechanism, in which case the progenitor star may still exist, and will be observed after the current outburst fades. The long-term monitoring of SN 2009ip, due to its proximity, has given the most extensive data set yet gathered of a high-luminosity interacting transient and its progenitor. It is possible that some purported Type IIn supernovae are in fact analogues of the 2012b event and that pre-explosion outbursts have gone undetected.

Key words: stars: massive – stars: mass-loss – supernovae: general – supernovae: individual: SN 2009ip.

1 INTRODUCTION

Stars with a zero-age main sequence (ZAMS) mass of greater than ~8 $M_\odot$ end their lives as core-collapse supernovae (CCSNe). The differing masses, metallicities and structures which these massive stars can have at the point of collapse give rise to a tremendous diversity of SN types. Among the most peculiar and extreme are the Type IIn (*narrow*) SNe (Schlegel 1990), which are typified by narrow (~100–500 km s^{-1}) emission lines of H, which arise from the collision of the SN ejecta with pre-existing dense circumstellar material (CSM; see Chevalier & Fransson 1994 for an overview of the theory of ejecta–CSM interaction).

Type IIn SNe are intrinsically rare, with relative rates (i.e. rates as a fraction of the total number of CCSNe) estimated to lie between 4 and 9 per cent (Smartt et al. 2009; Smith et al. 2011a). Their rarity is compounded by their diverse nature, with well-studied examples including long-lived events (SNe 2005ip and 2006jd; Fox et al. 2009; Stritzinger et al. 2012), events which show Wolf–Rayet features (SN 1998S; Liu et al. 2000; Fassia et al. 2001) and even a related family of events, of which the prototype was SN 2006jc, which show an interaction with a He-rich rather than H-rich CSM (Foley et al. 2007; Pastorello et al. 2007, 2008). Some Type IIL SNe have also shown evidence for an interaction with their environments at late epochs, for example SNe 1979C and 1980K (Fesen, Hurford & Matonick 1995; Fesen et al. 1999; Milisavljevic et al. 2012), while the Type IIn SN 1998S was shown to be still interacting with a dense CSM a decade and a half after explosion (Mauerhan & Smith 2012).

In some cases, Type IIn SNe have been linked to luminous blue variables (LBVs). LBVs are characterized by having bright absolute magnitudes ($M_{\rm bol} < -9.5$), irregular eruptions where they brighten by more than one magnitude, and a surface temperature during quiescence of between 12 and 30 kK (Humphreys & Davidson 1994). As Type IIn SNe require a dense circumstellar environment prior to explosion, a connection to LBVs – which shed large amounts of material into their CSM – seems natural.

The first connection between LBVs and Type IIn SNe was that eruptions of the former are often confused with the latter – a fact which led Van Dyk et al. (2000) to coin the term 'supernova impostors' to describe extreme outbursts of massive stars. While SN impostors share the key characteristics of Type IIn SNe, namely narrow emission lines signalling interaction, the crucial difference is that an SN impostor is a non-terminal event, whereas the progenitor star will not survive an SN explosion. The boundary between Type IIn SNe and impostors has been much debated in the literature [see, for example, SN 1961V (Zwicky 1961), which was revisited by Kochanek, Szczygiel & Stanek (2011) and Van Dyk & Matheson (2012), and the debated SN 1994W-like objects; Sollerman, Cumming & Lundqvist 1998; Dessart et al. 2009; Kankare et al. 2012. More recently, Humphreys et al. (2012) suggested that SN 2011ht was a giant eruption, while Mauerhan et al. (2013b) observed faint nebular SN lines, and instead proposed that SN 2011ht (and other SNe like it, which they termed IIn-P) was in fact a weak core collapse.

Direct evidence for an LBV–Type IIn SN link was found by Gal-Yam et al. (2007), who identified a source coincident with SN 2005gl in pre-explosion imaging, which was subsequently seen to have disappeared after the SN had faded (Gal-Yam & Leonard 2009). The bright absolute magnitude of the progenitor for SN 2005gl could only be matched by an LBV. Similar results from archival imaging have been found for SN 2010jl by Smith et al. (2011b). A physical connection between Type IIn SNe and LBVs was also made by Trundle et al. (2008), who observed multiple narrow absorption components for H and He in the spectrum of the Type IIn SN 2005gj, which they attributed to variable mass-loss in an LBV progenitor [although we note that Aldering et al. (2006) have proposed an alternative scenario, where SN 2005gj was a Type Ia SN exploding in a dense CSM].

In 2009 August, SN 2009ip was discovered close to NGC 7259 by the CHilean Automatic Supernova sEarch (CHASE) project (Maza et al. 2009). While the object was given an SN designation, it was rapidly realized that it was not a genuine SN, but rather an impostor (Smith et al. 2010a; Foley et al. 2011). Fortuitously, the site of SN 2009ip had been observed with the *Hubble Space Telescope* (*HST*) prior to the 2009 outburst, enabling Smith et al. and Foley et al. to identity a coincident point source with an absolute magnitude of $F606W = -9.8$, and consistent with a massive star of ~50–60 $M_\odot$. While the 2009 August eruption faded, SN 2009ip continued to suffer irregular outbursts over the following three years. Pastorello et al. (2013, henceforth P13) presented coverage of these eruptions, with a unique set of spectroscopic and photometric data, making SN 2009ip one of the best intensively monitored extragalactic transients to date. Remarkably, P13 found evidence for material accelerated to high velocities (~10^4 km s^{-1}) in 2011 September. The detection of fast material over one year prior to the 2012a and 2012b events – and at a point when SN 2009ip had *not* undergone core collapse – shows that high velocities cannot be taken as proof of a CCSN.

In 2012 July–August, SN 2009ip started a new phase of activity, as first reported by Drake et al. (2012). After an initial outburst which reached a peak absolute magnitude of $V = -14$ and lasted until around September 25 (termed the '2012a' event), SN 2009ip rapidly rebrightened to reach an unprecedented peak magnitude of $R = -18.5$ mag (the '2012b' outburst). P13, Mauerhan et al. (2013a) and Prieto et al. (2013) all published early photometry and spectroscopy of the eruption, which showed both signs of interaction (narrow lines) and broad absorptions in H and He, with velocities of up to 15 000 km s^{-1}.

In this paper, we present high-cadence ultraviolet (UV), optical and near-infrared (NIR) photometry of SN 2009ip, together with optical and NIR spectroscopy, covering the period from the peak of the 2012b event until the end of the observing season in 2012 December. The rest of the paper is organized as follows: in Section 2 we describe the observations obtained, and the reduction techniques used. In Sections 3 and 4 we characterize the photometric and spectroscopic evolution of the SN, and derive a bolometric light curve. Section 5 is devoted to simple modelling of the narrow H emission seen in SN 2009ip, which we use to derive densities for the CSM. Finally, in Section 6, we attempt to use our observational data and modelling to understand the evolution of SN 2009ip, and discuss whether the outbursts seen in late 2012 represent the final death of the star as an SN or rather an example of a non-terminal outburst. In all of the following, we adopt the foreground reddening and distance towards SN 2009ip quoted by P13 and others $\mu = 31.55$ mag, $A_R = 0.05$ mag. The distance adopted is also in agreement with that found by Potashov et al. (2013) from applying a geometric technique (the 'Dense Shell Method') to SN 2009ip itself.

2 OBSERVATIONS AND DATA ANALYSIS

Optical spectroscopic follow-up of SN 2009ip was chiefly obtained with the New Technology Telescope (NTT) + ESO Faint Object Spectrograph and Camera 2 (EFOSC2), as part of the Public European Southern Observatory (ESO) Spectroscopic Survey of Transient Objects (PESSTO).[1] The PESSTO data were supplemented with data from the Telescopio Nazionale Galileo (TNG) + Device Optimized for the LOw RESolution (DOLORES), and the Australian National University (ANU) 2.3 m telescope + Wide Field Spectrograph (WiFeS). Details of the instrumental configuration used for each spectrum are listed in Table 1. All spectroscopic data presented in this paper are available for download from the Weizmann Interactive Supernova data REPository (WISeREP; Yaron & Gal-Yam 2012).[2] All PESSTO data are also immediately publicly available from the ESO archive; high level data products will be available in 2013 June–July.

All long-slit spectra were reduced in the standard fashion, bias and overscan subtracted, flat-fielded using normalized lamp flats, wavelength calibrated to an arc lamp and flux calibrated to a spectrophotometric standard star. In the case of the EFOSC2 spectra obtained by PESSTO, these steps were carried out within the PESSTO pipeline,[3] while for the DOLORES spectra the reduction was performed within IRAF.[4] The PESSTO data were corrected for telluric

[1] www.pessto.org

[2] http://www.weizmann.ac.il/astrophysics/wiserep/

[3] The PESSTO pipeline has been developed by S. Valenti, and comprises a set of PYTHON scripts which call PYRAF tasks to reduce EFOSC2 and SOFI data.

[4] IRAF is distributed by the National Optical Astronomy Observatory, which is operated by the Association of Universities for Research in Astronomy

Table 1. Optical spectroscopy of SN 2009ip, together with the nominal resolution for each grating.

Date	Instrument	Grating	Res. (Å)
2012-09-22	ANU 2.3 m+WiFeS	B3000+R3000	2
2012-09-23	ANU 2.3 m+WiFeS	B3000+R3000	2
2012-10-08	NTT+EFOSC2	Gr#11,16	16
2012-10-09	NTT+EFOSC2	Gr#11,16	16
2012-10-14	NTT+EFOSC2	Gr#11,16	16
2012-10-15	NTT+EFOSC2	Gr#11,16	16
2012-10-20	NTT+EFOSC2	Gr#11,16	16
2012-10-22	NTT+EFOSC2	Gr#11,16	16
2012-10-22	TNG+DOLORES	LRB	11
2012-10-22	ANU 2.3 m+WiFeS	B3000+R3000	2
2012-10-23	ANU 2.3 m+WiFeS	U,B,R,I7000	1
2012-10-31	ANU 2.3 m+WiFeS	B3000+R3000	2
2012-11-04	NTT+EFOSC2	Gr#11,16	16
2012-11-07	NTT+EFOSC2	Gr#11,16	16
2012-11-12	NTT+EFOSC2	Gr#11,16	16
2012-11-14	NTT+EFOSC2	Gr#11,16	16
2012-11-19	ANU 2.3 m+WiFeS	B3000+R3000	2
2012-11-20	NTT+EFOSC2	Gr#11,16	16
2012-12-03	NTT+EFOSC2	Gr#11,16	16
2012-12-09	TNG+DOLORES	LRB+LRR	11,9
2012-12-11	NTT+EFOSC2	Gr#11,16	16
2012-12-20	NTT+EFOSC2	Gr#11,16	16

absorption by subtracting a model spectrum of the telluric bands, while the DOLORES spectra were corrected using a smooth spectral standard. For spectra where there were a significant number of cosmic ray hits, the LACOSMIC algorithm (Van Dokkum 2001) was used to identify and mask cosmic rays in the two-dimensional frames before extraction. The resolutions of the slit spectra were checked from the full width at half-maximum (FWHM) of narrow night sky lines, and were found to be $\sim$15 and $\sim$10 Å for the EFOSC2 and DOLORES data, respectively. These values are in good agreement with the expected resolution from the grating characteristics (reported in Table 1) and correspond to a resolution in velocity space (at the wavelength of Hα) of $\sim$500–700 km s^{-1}.

Some optical spectra of SN 2009ip were obtained with the WiFeS (Dopita et al. 2007, 2010) on the ANU 2.3 m telescope at Siding Spring Observatory in northern New South Wales, Australia. Observations were obtained with either the B3000/R3000 gratings, which provide wavelength coverage from 3500 to 9600 Å at a resolution of $\sim$2 Å, or the U/B/R/I7000 gratings which cover 3500–9100 Å with $\sim$1 Å resolution. As WiFeS is an integral-field spectrograph, the data were not reduced using the same techniques as for the rest of the optical spectra. Instead, data cubes for WiFeS observations were produced using the PYWIFES software,[5] and final spectra were obtained with a point spread function (PSF) weighted extraction routine.

NIR spectroscopy was obtained with the NTT+SOFI and Large Binocular Telescope (LBT)+LBT Near Infrared Spectroscopic Utility with Camera and Integral Field Unit for Extragalactic Research (LUCIFER) as detailed in Table 2. Solar analogues at a similar airmass were observed either before or after SN 2009ip, to facilitate the removal of the strong telluric absorptions which lie between 1 and 2 μm. For two epochs of NIR spectra (on November

(AURA) under cooperative agreement with the National Science Foundation.

[5] http://www.mso.anu.edu.au/pywifes/

Table 2. NIR spectroscopy of SN 2009ip.

Date	MJD	Instrument	Grating
2012-10-16	562 17.23	NTT+SOFI	BG+RG
2012-10-22	562 23.17	NTT+SOFI	BG+RG
2012-10-25	562 25.11	LBT+LUCIFER	zJ
2012-11-05	562 37.11	NTT+SOFI	BG+RG
2012-11-13	562 45.14	NTT+SOFI	BG+RG
2012-12-04	562 66.08	NTT+SOFI	BG+RG

13 and December 4), a flux standard was observed on the same night and used to calibrate the spectra, and for all other data the telluric standard was also used to flux calibrate SN 2009ip. The LUCIFER spectrum was reduced with the ad hoc pipeline of the LBT Spectroscopic Reduction Center of IASF-Milano, which includes bad pixel, dark and flat-field correction, optimal extraction, sky subtraction, and wavelength and flux calibration.

Optical photometry was obtained with the NTT+EFOSC2+ *U*#640, *B*#639, *V*#641, *R*#642, *i'*#705 (on the same nights as the EFOSC2 optical spectroscopy), with the Panchromatic Robotic Optical Monitoring and Polarimetry Telescope (PROMPT; Reichart et al. 2005) telescopes + *BVRI* on Cerro Tolodo and with the Liverpool Telescope + RATCAM + *u'BVr'i'*. In addition, regular photometry of SN 2009ip was obtained with the UltraViolet and Optical Telescope (UVOT) on board the *Swift* satellite (programme IDs 31486, 32579; P.I. Margutti). The PROMPT and RATCAM images were reduced automatically (trimmed, bias subtracted and flat-fielded) by their respective pipelines. Significant fringing was evident in the LT RATCAM *i'* images, and so a fringe frame was constructed from deep exposures of blank fields, scaled to match the science images, and subtracted from them. The EFOSC2 images were reduced using the PESSTO pipeline, again subtracting a smoothed fringe frame in *I*.

For the PROMPT and RATCAM data, PSF-fitting photometry was performed using the SNOOPY package within IRAF. SNOOPY is a PSF-fitting package using the routines in the DAOPHOT package, but specifically designed for SN photometry, and including several additional functions such as artificial star tests to estimate photometric errors. The zero-point for each image was determined from aperture photometry of the sequence stars listed in P13, while the same colour terms as used by P13 were applied to the instrumental magnitudes. The smaller field of view of EFOSC2, coupled with the short exposure times necessary to avoid saturating the bright target, resulted in only a single reference star bring present in the images obtained in October. As this is insufficient to build a PSF for each frame, we performed aperture photometry on these data. As for the PROMPT and LT data, the zero-point for each night and filter was determined from local sequence stars, while colour terms for EFOSC2 were evaluated from observations of Landolt standard fields on three photometric nights. All optical photometry, calibrated to the Landolt photometric system, is reported in Table B1.

The *Swift* UVOT frames were reduced using tools within HEASOFT.[6] Individual images for each epoch were first co-added before aperture magnitudes were measured following the prescription of Poole et al. (2008). To transform the UVOT *ubv* magnitudes from the instrumental system into standard *UBV* Johnson magnitudes, shifts of $\Delta U = 0.270$, $\Delta B = 0.018$ and $\Delta V = -0.042$ mag were applied. These shifts were computed from the magnitudes of

---

[6] Available from the NASA High Energy Astrophysics Science Archive Research Center.

the reference stars in the SN field and are consistent with those reported in P13. These corrections have been applied to all UVOT magnitudes and the resulting magnitude values are reported in Table B1. The *uvw2, uvm2, uvw1* magnitudes are reported in Table B2 in the UVOT photometric system.

NIR imaging of SN 2009ip in *JHKs* was obtained with the NTT + SOFI, the LBT + LUCIFER and the Nordic Optical Telescope + NOTCAM. Multiple, dithered, on-source images were taken in each filter; these images were then flat-fielded and median-combined to create a sky frame. The sky frame was then subtracted from each of the individual images, which were then aligned and co-added. For the LUCIFER imaging, these steps were carried out with the pipeline at the LBT Imaging Data Centre at the Observatory of Rome. Aperture photometry was performed on SN 2009ip, taking care to avoid any flux from the nearby foreground star to the north. Zero-points for each image were determined from aperture photometry of the same sequence stars as used for the optical photometry, calibrating them to their 2MASS *JHK* magnitudes. The *K* and *Ks* filters are slightly different, which has a negligible effect on our photometry. NIR magnitudes for SN 2009ip are reported in Table B3.

3 SPECTROSCOPIC DATA

The full set of spectra collected for SN 2009ip is presented in Tables 1 and 2. In general, the spectra are blue at early times, and are dominated by narrow emission lines from H and He I. As the SN evolves, broad ($\sim 10^4$ km s^{-1}) absorptions appear in the Balmer lines, while the [Ca II] NIR triplet emerges in emission, along with Na I D. We do not observe a transition to a nebular SN spectrum; indeed the last spectrum in our data set appears to resemble most closely the spectrum of SN 2009ip from 2009 September, with the same lines present at both epochs, albeit at higher velocities in 2012. In Sections 3.1 and 3.2, we describe in detail the spectroscopic evolution of SN 2009ip.

3.1 Optical spectroscopic evolution

3.1.1 September 22–September 23

The first spectrum in our sequence (from September 22) as shown in Fig. 1 is contemporaneous with the TNG+DOLORES spectrum presented in P13, coinciding with the end of the 2012a eruption, and immediately prior to the start of the 2012b event. As this spectrum is effectively identical to the one obtained on the following night (September 23), these two spectra will be discussed together. The most prominent features in the spectra are the Balmer lines. At the rest wavelength of Hα, SN 2009ip has a narrow (FWHM $\sim$ 500 km s^{-1}) emission component superimposed on broad emission (FWHM $\sim$ 6000 km s^{-1}). A P-Cygni absorption trough is also present with a minimum at -7500 km s^{-1} with respect to the rest wavelength of Hα. This absorption is weaker than the broad emission. The higher Balmer lines, notably Hβ and Hγ, have similar multicomponent profiles, but with a stronger broad absorption compared to the broad emission. The minimum of the broad absorption in Hβ is also at a lower velocity than that seen in Hα. A 'shoulder' of emission is also visible in the blue wing of Hβ and Hγ (at a velocity of -1800 km s^{-1}), which is less visible in Hα. The He I 5876 Å line which appears later is absent at this phase. Metals are present as narrow emission lines, including the blended Na I D lines at 5890 and 5895 Å, weak Ca II NIR triplet lines and numerous Fe II lines such as multiplets 27 and 42.
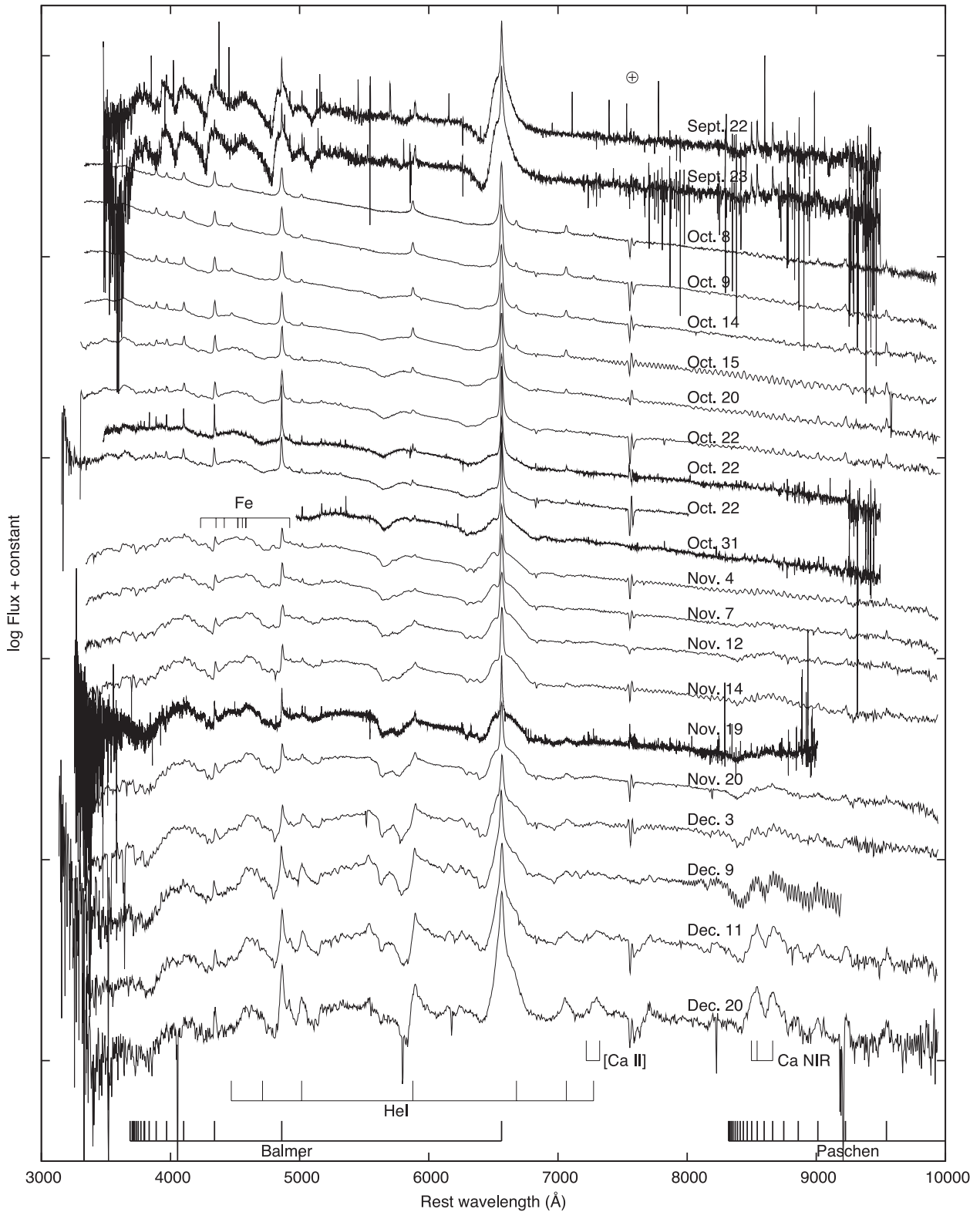
Figure 1. The sequence of the optical spectra of SN 2009ip, as detailed in Table 1. Note that the high-resolution spectrum obtained on October 23 is not included here, but is shown separately in Fig. 3. The wavelength of residuals from the telluric correction is indicated with ⊕.

3.1.2 October 8–October 15

The October 8 and 9 spectra were obtained when SN 2009ip was at the peak of the 2012b event. The spectra have a blue continuum and

are dominated by narrow (unresolved, $<700 \, \mathrm{km \, s^{-1}}$) Balmer emission. The Paschen series are also visible at wavelengths $>8500 \, \text{Å}$ although with much weaker emission. The narrow central component of Hα, together with the broad base of the line, is well fitted
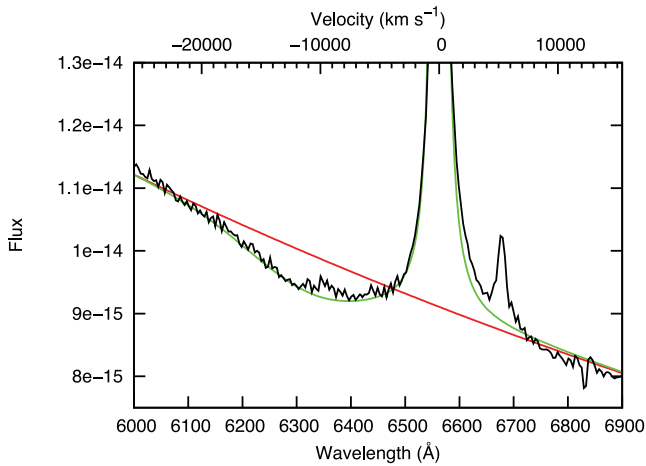
Figure 2. The region of Hα in our October 8 spectrum of SN 2009ip, showing the shallow broad absorption. In red is a blackbody fit to the continuum, while in green is the same blackbody, with a Lorentzian line of FWHM 17 Å and a Gaussian absorption with FWHM 270 Å superimposed. The Lorentzian plus continuum is an excellent fit to the red wing of Hα (with the exception of He λ6678), whereas in the blue wing there is an apparent absorption which is fitted by the Gaussian. As discussed in the text, it appears that the absorption may have two components, although a single Gaussian (as shown here) also gives a reasonable fit. The second *x*-axis shows the velocity with respect to the rest wavelength of Hα.

by a Lorentzian with an FWHM of 750 km s⁻¹. The broad absorption is still present, but much weaker than in the previous epoch. We show in detail the Hα line profile in Fig. 2, together with a Lorentzian fit, clearly showing the broad shallow absorption in the blue. Tantalizingly, the profile appears to resemble the multicomponent absorption we see at later epochs, and we obtain a best fit to the absorption component with two Gaussians with minima at −6000 and −12 000 km s⁻¹. However, as the feature is weak we cannot formally exclude a single broad absorption. He I λ5876 is the strongest line after the Balmer series; it has a similar Lorentzian profile to Hα (narrow emission on a broad base, together with a hint of broad absorption in the blue). Other weaker He I lines are detected at 4471, 4713, 5015, 6678 and 7065 Å, and tentatively at 7276 Å. We see no lines from He II (for example at 4686 Å), nor of the Ca NIR triplet or Na I D.

The next spectra in our sequence are from October 14 and 15. These spectra are similar to those obtained on October 8 and 9, but with a double absorption in the Balmer lines. Fitting two Gaussians to the absorptions in Hα, we find velocities of −8000 and −12 500 km s⁻¹. Interestingly, while Hβ and Hγ appear to have the same double absorption as Hα, the lower velocity component is at only ∼4000 km s⁻¹. The higher velocity component is difficult to measure accurately due to the steep continuum, but it also seems to be lower than in Hα. He I 5876 Å has a similar narrow Lorentzian emission component to the preceding epoch, but now also has a clear broad absorption centred on −12 500 km s⁻¹. This absorption does not appear to have the two-component structure seen in the Balmer lines, but is instead well fitted by a single Gaussian absorption. The broad absorption is not seen in the other He I lines, but as these are much weaker than He I 5876 Å this is perhaps not surprising. While an alternative source for the broad absorption could be Na, this would imply a velocity of 13 500 km s⁻¹, which is uncomfortably higher than Hα.

3.1.3 *October 20–October 23*

On October 22 we obtained the spectra of SN 2009ip from three different telescopes, all of which are similar to that obtained two days earlier on October 20. At this phase, the narrow emission on a broad base in Hα can no longer be fitted with a single Lorentzian profile. Instead, we find that we need two components to fit the emission, one narrow (FWHM ∼ 800 km s⁻¹) and one broad (FWHM ∼ 10 000 km s⁻¹). The broad emission is not symmetric, as a 'shoulder' of emission is present in the blue wing of Hα which is not present in the red. While the broad absorption can be reasonably fitted with a single Gaussian at −10 000 km s⁻¹, if we take the position of the two absorption components from the previous epoch, then we can see two notches still present at velocities of ∼8000 and 12 000 km s⁻¹. Hβ has a similar broad absorption to Hα, but with a much less pronounced broad emission, while in Hδ the broad emission is absent. For He I, the narrow emission is much weaker than in previous epochs, and there is no strong broad emission, while we still see a strong absorption at −11 000 km s⁻¹ in the 5876 Å line. At this phase, we also see the emergence of a broad emission feature at ∼4500 Å with an FWHM of ∼10 000 km s⁻¹. It is difficult to judge the strength of the 4500 Å feature, as it is bracketed by the broad absorption of Hβ and Hδ, which serve to lower the apparent level of the continuum. While this feature was present during October 14 and 15, it was much weaker and was plausibly associated with the He 4471 Å line. However, for the 4500 Å line to be caused by He I on October 22 would require the peak of the emission to be redshifted by ∼2000 km s⁻¹. More problematically, it is difficult to see how we could get emission in the 4471 Å line, without corresponding emission in the 5876 Å He line. While there are no strong, low-ionization state lines arising from any intermediate-mass elements around 4500 Å, we note that in Type II SNe an emission feature at this wavelength is often seen at early times, arising from multiple blended Fe I and Fe II lines such as multiplets 37 and 38. The Fe which gives rise to this in SNe is primordial, so it is entirely possible that we could see a similar feature in a massive non-terminal eruption of an LBV. We also see two emission lines (FWHM ∼ 50 Å) in the extreme blue end of the spectrum, at 3490 and 3650 Å. The 3650 Å feature may be caused from the combined flux of the higher order Balmer lines (10–2 transitions and higher), as the series converges to this wavelength, and the blue edge of the line corresponds to the wavelength at which the separation between the lines becomes lower than the instrumental resolution of EFOSC2 (for comparison we can clearly resolve the $H_{J=9-2}$ line in the same spectrum). The identity of the 3490 Å line is uncertain, although as for the ∼4500 Å bump, it may be attributable to blended Fe emission.

We obtained a higher resolution spectrum of SN 2009ip on October 23 with WiFeS using the $R = 7000$ gratings (Fig. 3). We measured an FWHM of the narrow Lorentzian emission in Hα of 266 ± 13 km s⁻¹, 243 km s⁻¹ in Hβ and 242 km s⁻¹ in Hγ. As the FWHM is larger than the instrumental resolution of WIFES (45 km s⁻¹ at Hα), we adopt their mean (250 ± 11 km s⁻¹) as the velocity of the CSM. The 3650 Å feature is indeed seen to be comprised of a large number of Balmer lines, as the blue edge of the bump seen in the spectra from October 22 is resolved out into a blend of the Balmer lines with upper levels between $J = 13$ and 22. The other striking feature is the appearance of a large number of weak, narrow emission lines from Fe. These features are not seen in the lower resolution data from the preceding night, but were present in the spectra of earlier eruptions obtained with XShooter by P13. Unfortunately, we do not observe the auroral O
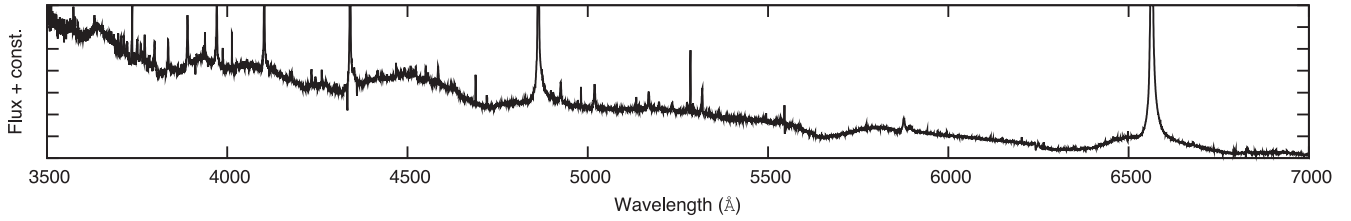
Figure 3. The highest resolution spectrum of SN 2009ip in our data set, taken on October 23 with the U7000, B7000, R7000 and I7000 gratings on WiFeS, showing the forest of narrow Fe emission lines.
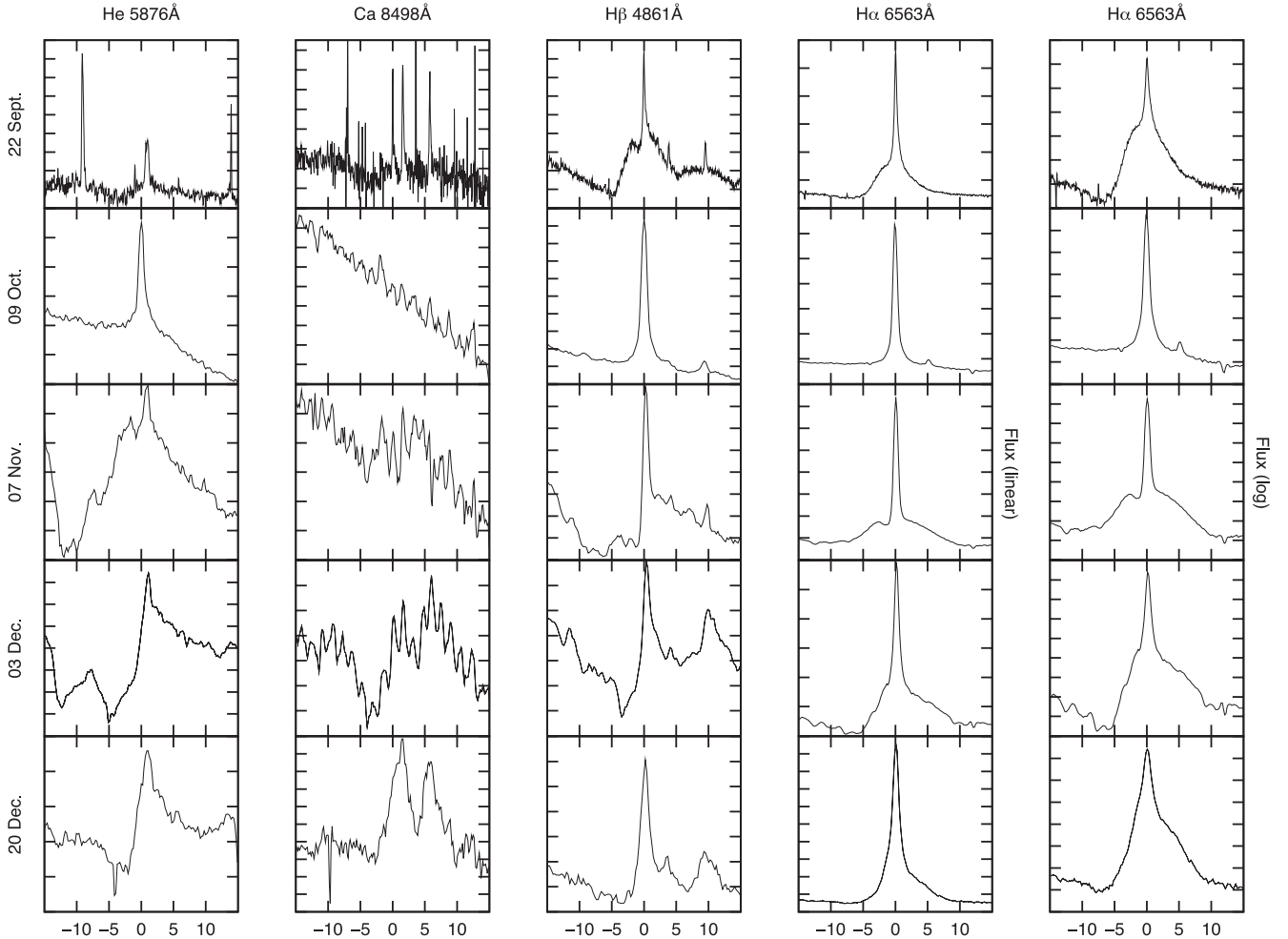

Figure 4. The evolution of the line profiles for selected elements in SN 2009ip. All panels are on a common velocity scale, centred on the rest wavelength of the line in question, with units of 10^3 km s^{-1}. From top to bottom, the rows correspond to: pre-2012a outburst (September 22), peak 2012a outburst (October 9), first 'bump' in the light curve (November 7), approximately two months past peak (December 3) and the latest spectrum (December 20). All plots are on a linear flux scale, normalized to the peak of the line in question, with the exception of the column on the far right, which shows the Hα line on a logarithmic scale to emphasize the structure at the base of the line.

line at 5007 Å precluding a direct estimate of the metallicity of the environment.

3.1.4 October 30–November 7

In the spectra obtained on October 30 and November 04, Hα has quite distinct narrow and broad emission features. The former has an FWHM of $\sim$700 km s^{-1}, while the latter has an FWHM of $\sim$ 10 000 km s^{-1}. The broad absorptions seen at earlier epochs are still present, with multiple components at 12 500 and 10 000 km s^{-1}. We

note however that the broad absorptions are weaker than the corresponding broad emission by a factor of a few. The blue shoulder in Hα which was beginning to appear in the October 22 spectrum is more evident; this feature can be seen in velocity space in Fig. 4. If it is caused by an additional emission component, then it consists of material moving at a velocity of -3000 km s^{-1} with respect to the narrow component, and with an FWHM of $\sim$1500 km s^{-1}. Alternatively, the feature could be viewed as an absorption centred on -1500 km s^{-1}, although this is perhaps less likely, as it would imply that the strong broad emission is intrinsically quite asymmetric. The absorption velocity of the feature could be associated with

fast CSM material at 1500 km s^{-1}, although it is difficult to explain in this case why the feature was not also seen at earlier epochs. Hβ and Hγ do not show as strong narrow emission when compared to Hα. The broad features in Hβ and Hγ are also quite peculiar. For both lines, the broad emission seen strongly in Hα is absent, while the broad absorption is much more pronounced. We see multiple absorptions, with the highest velocity minimum at $-12\,500$ km s^{-1} in Hβ, but with the bulk of the absorption at -8000 km s^{-1}. We also see for the first time in the 2012b event clear absorptions from ejecta at quite low velocities, with the first minimum in Hβ at only -2000 km s^{-1}. The strong absorption at 5660 Å which we attribute to He I with a velocity of $-11\,000$ km s^{-1} is still present, without any clear corresponding broad emission. However, the narrow He I 5876 Å line has now vanished, and has been replaced with a re-emergent Na I D line at 5890 and 5895 Å suggesting that from this point onwards we cannot be confident that the broad feature is solely caused by He. We also observe the re-appearance of narrow Fe lines in the spectrum of SN 2009ip, such as the 5167 Å line from multiplet 42.

The spectrum of SN 2009ip from November 7 is similar to those discussed in the preceding paragraphs. Hα now has a clear, three-component absorption, with minima at $-12\,500$, $-10\,000$ and -6500 km s^{-1}. The absorption in Hβ now begins even more sharply at a velocity of only -1000 km s^{-1}. Most interestingly, however, is the confirmation of a two-component absorption in the line at 5660 Å. If the line is still dominated by He, then the velocities of the two absorptions are 6000 and 11 000 km s^{-1}, while if Na is dominant, the velocities are slightly higher at 12 000 and 7000 km s^{-1}. Only the Na I D narrow emission is present (albeit weakly), but it is probable that the broad emission is a combination of both He and Na. At this epoch, we also start to see the emergence of a bump around 8500 Å which will develop into the Ca NIR triplet in later spectra. In the blue part of the spectrum, while line identifications are difficult given the complicated velocity structure of the outburst, a broad emission line at $\sim$4100 Å appears to be present, which we tentatively identify as a blend of Fe II lines.

3.1.5 November 12–November 20

By November 12, the 'shoulder' in the blue wing of Hα has begun to fade. We again fit the emission in Hα with a narrow and a broad Gaussian, the former is centred on the rest wavelength, while the latter is shifted by 1000 km s^{-1} to the red and has an FWHM of $\sim$10 000 km s^{-1}. The majority of the flux in Hα is now emitted by the broad component, while the broad absorptions (which are by now extremely shallow) persist at $-12\,500$, $-10\,000$ and -6500 km s^{-1}. The overall shape of the absorption in Hα is flat and shallow, a shape which is mirrored in Hβ. We also see the emergence of two emission lines at 5021 and 7075 Å. While both these features are weak (and so their centres are uncertain), if these are the He I 5015 and 7065 Å lines, then they are both systematically redshifted by several hundred km s^{-1}. This is in contrast to Hα, which is within $\sim$1 Å of its rest wavelength. We also see what appears to be a broad bump in the spectrum at $\sim$5250 Å, to the red of the probable He line. Superimposed on this bump are numerous weak Fe emission lines, indicating that this could be from Fe. In the probable He/Na blend at 5660 Å, the redder absorption component which emerged on November 7 is now comparable in strength to the other absorption. The Ca NIR triplet is clearly emerging in the red part of the spectrum, with high velocities and an apparent P-Cygni profile.

On November 20, the complex Hα structure persists with absorption up to $-12\,500$ km s^{-1}, Hβ is largely unchanged from the preceding spectrum. For Hδ, the expected absorption is masked by the Fe II line at 4100. The narrow He emission grows in intensity, as does the Ca triplet. Most interestingly, the possible Na/He feature at $\sim$5700 Å now has two clearly separated absorption minima which are well fitted by Gaussians, one centred at $-13\,000$ km s^{-1} and one at -6500 km s^{-1}. The narrow emission is still located at the expected position for the unresolved Na I D lines. An apparent absorption feature emerges at 5123 Å, although at this phase it is very difficult to locate the continuum, and we suggest that this is only an apparent absorption caused by the strengthening of the probable Fe bump within $\sim$5150–5550 Å, which was first seen in the November 12 spectrum.

3.1.6 December 3–December 11

By December 3, the broad base of the Hα line has become quite asymmetric, with significantly more flux in the red wing compared to the blue. The narrow emission in Hα and Hβ is markedly weaker by this epoch, while Hδ is nearly completely gone. Interestingly, the highest velocity absorption in Hα, at $\sim$12 000 km s^{-1}, appears to be weakening. Ca NIR continues to strengthen, with a clear absorption which has a minimum at -3500 km s^{-1} relative to the bluemost component of the triplet (8498λ). We see the emergence of narrow emission features at 6159 and 7313 Å which are probably Fe.

On December 11, the spectrum is quite similar to that from December 3, with the most significant changes being the appearance of [Ca II] at 7219 and 7323 Å and the re-emergence of strong Paschen lines with an FWHM of $\sim$1500 km s^{-1}.

3.1.7 December 20

The last optical spectrum we obtained of SN 2009ip was on December 20. We fit the profile of Hα with a narrow Lorentzian emission with an FWHM of 1200 km s^{-1} and a broad Gaussian emission with an FWHM of 8500 km s^{-1}. The centre of the broad component is offset by 800 km s^{-1} to the red to reproduce the asymmetric emission. The absorption component is weaker than at previous epochs, and has a blue edge at $-11\,000$ km s^{-1}. The [Ca II] emission at 7219 and 7323 Å continues to grow stronger, becoming comparable in strength to the He I 7065 Å line. Meanwhile, the P-Cygni profile in the Ca NIR triplet has disappeared, to be replaced with a line purely in emission, which resembles that of a late-time nebular SN line. What is most striking about the final spectrum of SN 2009ip is the resemblance to the spectra of the transient taken three years previously in 2009. A comparison is shown in Fig. 5. All the lines present in 2009 September are also visible in the 2012 December spectrum, with the only difference being much higher velocities in the latter. The continuum is somewhat redder in 2012. H, He, Ca, Na and Fe are all present, but we see no evidence for freshly nucleosynthesized materials. There is no sign of [O I] at 6300 and 6364 Å, and although the emission could be speculated to fill in some of the absorption in Hα, we see the same profile in Hβ and Hα, indicating that this is not the case. The two faint emission lines visible to the blue of Hα are from multiplet 74 of Fe II. Strong Mg I] 4571 Å does not appear to be present either, although the presence of Fe emission in this region of the spectrum makes this a less secure result. However, the lack of clear Mg I] 4571 Å is in accord with the absence of the 1.5 μm line in the NIR. We also see the emergence of a line at $\sim$7710 Å, from December 11
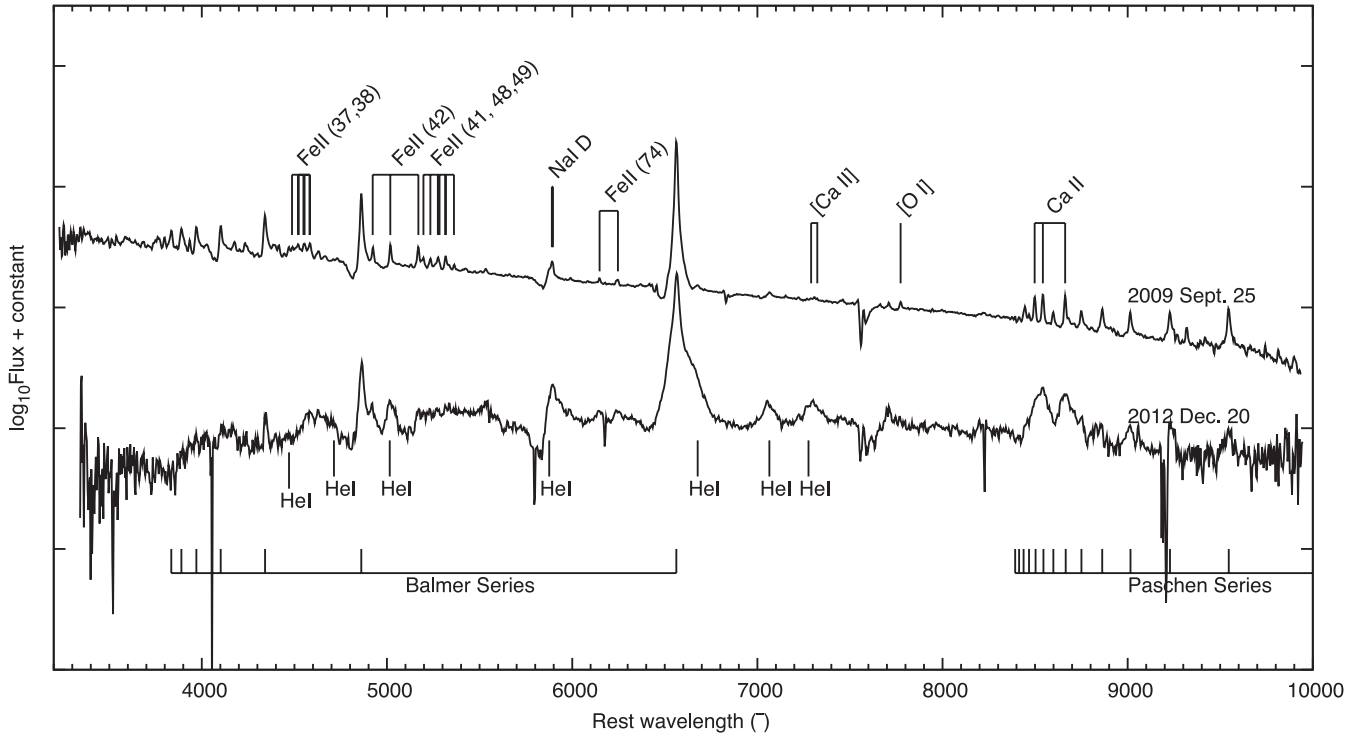
Figure 5. Comparison of the 2009 September spectrum of SN 2009ip presented by P13, and the final spectrum we obtained in 2012 December. The same lines are present at both epochs, albeit with higher velocities in 2012. In general, the spectra are quite similar, although we note that the Ca and [Fe] emission is more pronounced in 2012. In addition, the main lines identified are labelled.

onwards. While the residual from the telluric *A* band contaminates this region of the spectrum, the line does appear to be real; however, its wavelength is offset by −60 Å from O I 7774. The continuing presence of strong He I emission at this epoch is striking, and could provide further evidence that interaction is a significant source of energy, as photoionization will probably be too weak to support these lines. The strong He lines may also suggest an overabundance of He, although detailed chemical modelling is required to confirm this.

In Fig. 6 we compare the spectral evolution of SN 2009ip to that of a sample of interacting SNe, ranging from the weakly interacting Type II SN 2007pk through to the well-studied Type IIn SNe 1998S and 2010jl (Fassia et al. 2001; Inserra et al. 2012; Zhang et al. 2012). Spectra of SNe 1998S and 2010jl were obtained from the WISeREP.[7] The best match is the +97 d spectrum of SN 1998S, which is quite similar to the +124 d spectrum of SN 2009ip. However, Ca is much stronger in SN 1998S, while the He lines are weaker compared to SN 2009ip.

3.2 NIR spectroscopy

Aside from the optical spectroscopy, we obtained a sequence of NIR spectra of SN 2009ip as shown in Fig. 7. These spectra are dominated by H, with clear detections of the Paschen lines and Brγ at all epochs. We also see strong He emission at 1.08 μm, and more weakly at 2.06 μm. Besides these elements, there are no other lines present. Most notably, we see no signs of O in the *J*-band region, while Mg at 1.5 μm is similarly absent. The spectra do not show any change in their slope over the period between October 16 and

December 20, in agreement with the flat $J - H$ and $H - K$ colours seen in Fig. 15.

Our highest resolution NIR spectrum is taken with LBT+LUCIFER on October 25, and is shown in detail in Fig. 8. Paβ and γ have an FWHM of 330 km s^{-1}, slightly higher than the narrow component of the Balmer lines in the optical. Interestingly, we see a structure in the blue wing of the Pa lines, with emission components at velocities of −1950 and −1550 km s^{-1} relative to Paγ and δ, respectively. This structure, which is not visible in the preceding or following SOFI spectra, is contemporaneous with the emergence of the blue shoulder in Hα in the optical. We note, however, that the blue shoulder in the optical spectra was present at velocities of ∼3000 km s^{-1}, higher than what is seen in the NIR. We also find evidence for a weak P-Cygni absorption in Paδ and possibly Paβ, with minima of −3000 km s^{-1} for the former, but only −900 km s^{-1} for the latter. The minimum in Paβ is much lower than that observed in other lines, and is comparable to the typical velocities seen in LBV outbursts. We must caution, however, that the S/N is not as good here as at shorter wavelengths, and so the identification of this component is more tenuous.

We see a broad absorption at 1.043 μm, which has a velocity minimum of 14 500 km s^{-1} with respect to Paγ. We do not see a corresponding minimum in Paβ or δ, and so we consider it more likely that this is associated with the strong He I line at 1.083 μm, in which case the absorption minimum lies at 11 500 km s^{-1}. This is similar to what we measure in the Na/He blend in our optical spectra from October 30.

3.3 The line profiles of SN 2009ip

The H and He lines in SN 2009ip are characterized by narrow emission on a broad base, and multiple broad absorptions at velocities
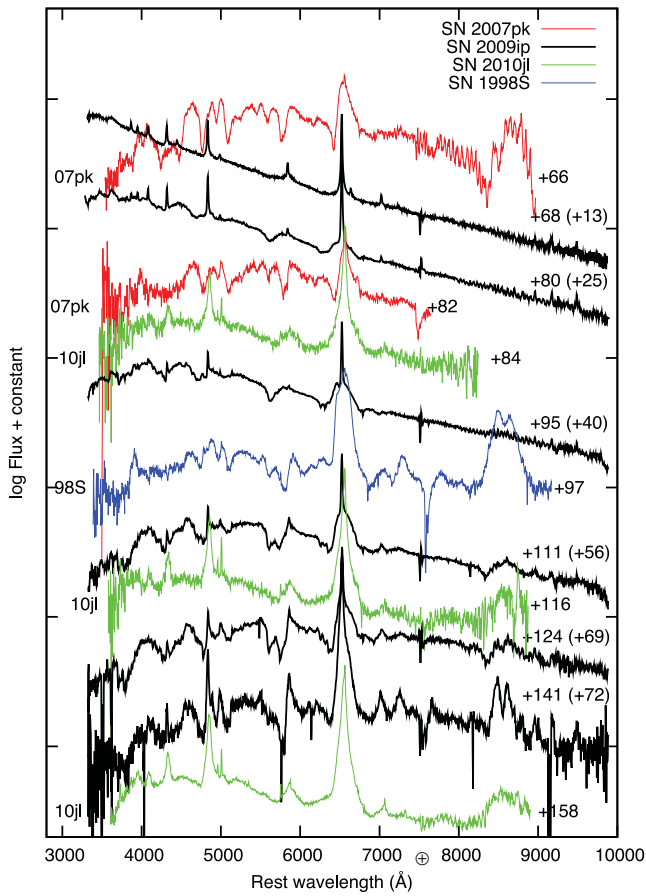
Figure 6. Optical spectra of SN 2009ip at representative epochs, compared to a sample of Type IIn SNe. Data are from Fassia et al. (2001), Zhang et al. (2012) and Inserra et al. (2012). The phase of each spectrum is indicated in the plot; for the spectra of SN 2009ip the phase from the start of the 2012a event (August 1) is given, together with the phase from the start of the 2012b event in parentheses.

of the order of 10^4 km s^{-1}. Below we discuss each component of the Balmer lines in turn.

3.3.1 Narrow H emission

Similar to what is observed in an H II region, the narrow lines arise from the CSM. While the H in an H II region is ionized from massive OB stars, in the case of Type IIn SNe the CSM is ionized by either the flux of the SN and/or the emission of the cool dense shell. The velocities in the narrow lines ($\sim$500 km s^{-1}) are similar to that seen in many Type IIn SNe and LBVs (Kiewe et al. 2012), although lower than those seen in some extreme examples of the class of SN impostors (Pastorello et al. 2010). The narrow lines are present at all epochs in SN 2009ip, although they are decreasing in strength with respect to the broad component over the period of the 2012b event. We see no narrow P-Cygni absorption in Hα from a wind, as shown in Fig. 9. This is in contrast to the sample of interacting SNe studied by Kiewe et al. (2012).

We measured the central wavelength of the narrow component in Hα in all our spectra by fitting a Gaussian to the line, excluding the broad base from the fit. A plot of central wavelength as a function of time is shown in Fig. 10, which reveals a small but significant trend towards redder wavelengths with time.

The slight shift of the narrow component of Hα to redder wavelengths is unusual, although we note that a similar effect was seen by Kankare et al. (2012) in SN 2009kn. A shift to the *blue* could be easily explained by the formation of dust in the ejecta. While one may invoke dust destruction to explain the opposite effect, the shift to the red is quite gradual and does not appear to coincide with the peak of the UV flux which might be expected to destroy the dust. Furthermore, if there were also significant dust being destroyed, an NIR infrared excess which disappears over time would also be expected, although we do not observe this in our photometry. Dust formation in a clump of material moving towards the observer could be an alternative explanation, although we do not see a strong NIR excess in our photometry which may be associated with dust formation.

3.3.2 Broad emission

The broad emission is approximately centred on the rest wavelength of Hα. While broad emission is usually associated with emission from ejecta at a large velocity, Chugai (2001) first suggested for the Type IIn SN 1998S that an alternative explanation could be scattering of photons; a similar result was found by Dessart et al. (2009) for SN 1994W. Repeated Thomson scattering of photons by electrons in the dense CSM can give rise to broad lines which have a Lorentzian profile, which can be seen most clearly in the October 8 spectrum of SN 2009ip. An alternative mechanism to create broad lines is boxy emission from interaction, as noted by Chevalier & Fransson (1994).

The broad emission becomes notably asymmetric after November 4, approximately coinciding with the first bump in the light curve. This raises the possibility that the bump is due to the ejecta encountering a denser region of CSM expelled by the progenitor star. If the density is not uniformly enhanced in all directions, then we may expect asymmetries to arise in the profile of Hα.

3.3.3 Broad absorption

We see broad absorption extending out to a velocity of $-16\,000$ km s^{-1}, with a flat bottomed profile. While a shallow, flat-bottomed absorption trough is unusual in SN and LBVs, it can be explained by the presence of a thin shell of absorbing material (Jeffery & Branch 1990). Interestingly, Jeffery & Branch find that in such an arrangement the maximum absorption in the line is 20 per cent of the flux in the continuum, which is in good agreement with what we see in the Hα trough in the EFOSC2 spectrum from November 14.

The presence of the broad Hα absorption in the spectrum at peak (Fig. 2) indicates that the optical depth of the cool dense shell cannot be much greater than a few. Alternatively, we require a clumpy CSM–ejecta interaction, where the high-velocity ejecta is visible through windows in the cool dense shell, and which could be caused by instabilities in the ejecta (Chevalier, Blondin & Emmering 1992).

A final interesting point of note in SN 2009ip is that the broad absorption appears stronger in Hβ than Hα. This is in contrast to what is expected, given that the optical depth in Hα is always higher than in Hβ. A possible explanation for this could be broad Hα emission 'filling in' some of the absorption in Hα. At high densities, Hβ is quenched as the $n = 4$ level is depopulated to $n = 2$ via Paα. In this case, one would also expect to see strong Paα
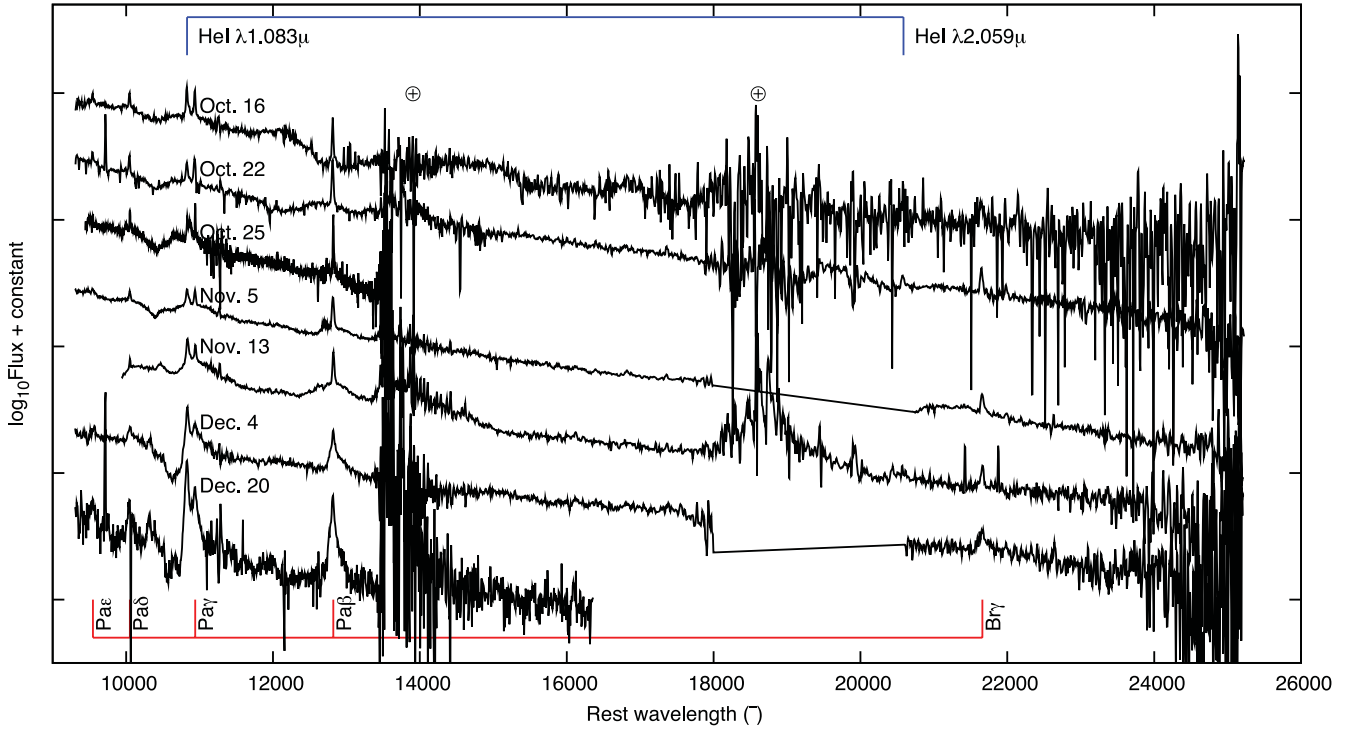
Figure 7. The sequence of the NIR spectra of SN 2009ip. Regions of strong telluric absorption where the S/N of the spectrum is poor are indicated with an ⊕ symbol; the rest wavelengths of the H and He lines visible in the spectra are also indicated.
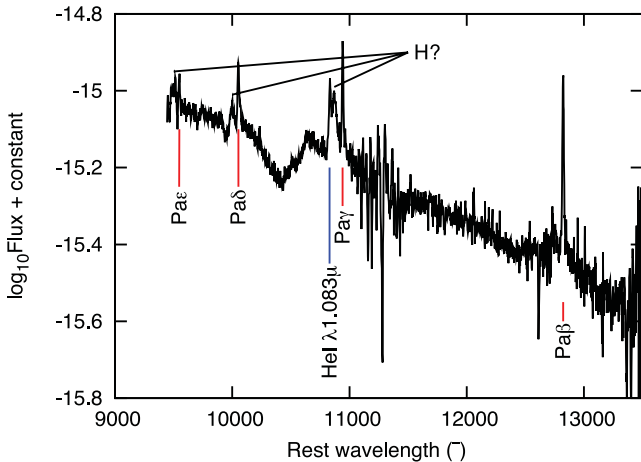

Figure 8. Close-up of the LUCIFER spectrum described in the text, with the emission components in the blue wing of the Paschen lines indicated.

Figure 9. Hα from our highest resolution spectrum, obtained on October 23. We see no evidence for a narrow ($\lesssim 250\,\mathrm{km\,s^{-1}}$) P-Cygni absorption at high resolution.

emission, but as this line is in the telluric band at 1.87 μm, it is difficult to test this hypothesis.

4 PHOTOMETRY

4.1 Light-curve evolution

The photometry of the 2012a event, together with the initial rise of the 2012b event, has been presented by P13. There is some overlap between these data and our first photometry obtained from NTT+EFOSC2. We find excellent agreement with the magnitudes reported by P13 in the region of overlap (Fig. 11); both sets of photometry agree to within their uncertainties, and show no systematic offsets. We have also compared our light curve to the *BRI*
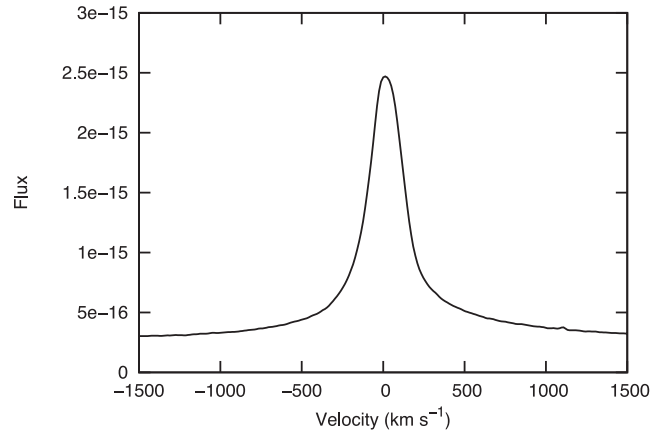
data presented by Mauerhan et al. (2013a), and find in general fair agreement between the two data sets within the uncertainties, and again see no systematic offset. The region of the bump in the light curve (around November 7) is the only discrepancy, where Mauerhan et al. find a similar increase in *I*, a larger increase in *B* and no increase in *R*, although the reason for this disagreement is unclear.

The light curve in all filters exhibits a decline from the bolometric maximum of the 2012b event (around October 3, MJD 562 03) until the end of the observing season on December 29 (MJD 562 90) when SN 2009ip disappeared behind the Sun. The decline is the strongest in the UV bands, with a drop of 8 mag from peak in *uvw*2 over 50 d, compared to only a 2 mag drop over the same period in *I*. During our last observation of SN 2009ip, taken on December 29 in *V*, the transient had faded to $M_V = -13.1$, 5 mag below peak. Even at
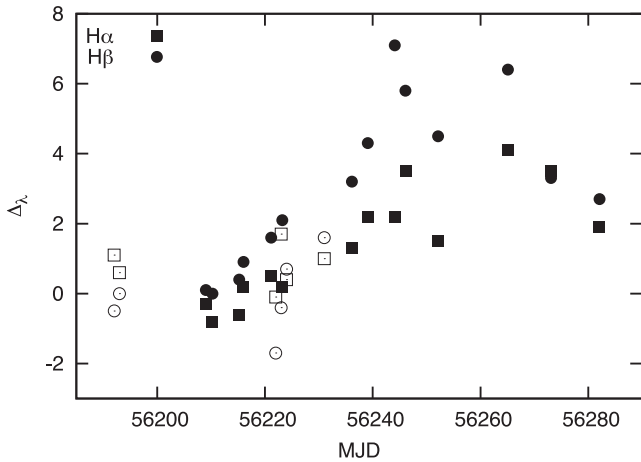
Figure 10. Wavelength shift of the narrow components of Hα and Hβ, relative to the rest frame of NGC 7259. The filled points indicate measurements obtained from the EFOSC2 spectra, which were pipeline reduced in a homogeneous fashion and had their wavelength calibration checked against night sky lines. The open symbols indicate measurements made on spectra from TNG+DOLORES and the ANU 2.3 m+WiFeS.

this phase the SN is still 4.5 mag brighter in *R* than the quiescent magnitude reported by Foley et al. (2011), *F*606*W* = 21.84 ± 0.17.

Around November 1, we see a clear bump in the light curve of SN 2009ip, where the transient brightens by 0.2–0.5 mag in all filters. Curiously, the bump appears to develop first in the redder filters. We show a zoomed-in section of the light curve of SN 2009ip
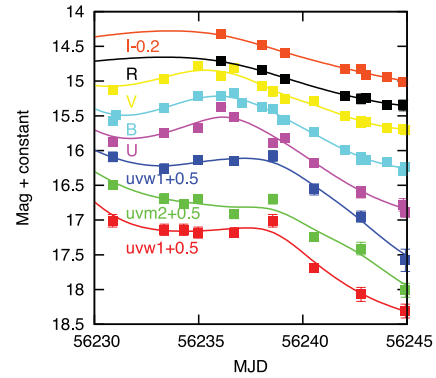

Figure 12. The region of the first bump in the light curve of SN 2009ip (around November 1), along with spline fits to the data.

in Fig. 12, where we have fitted natural splines to the photometric points between MJD 562 30 and 562 45 in each filter (taking the points immediately prior and subsequent to this range as the boundary values, and weighting all points equally). From the spline fits it appears that the bump becomes visible first in *R* and *I*, and lags by a few days in the *Swift* UV filters. The bump also appears to be more pronounced in the optical; while we have probably missed the peak in *RI*, *UBV* shows a clear rise, as opposed to *uvw*1, *uvm*2, *uvw*1 which merely flatten for a few days.

A second bump in the light curve can be seen at the start of December (MJD ∼562 65). This bump is less pronounced than the one seen around November 1, with the optical bands merely flattening for a period of around a week, rather than increasing in
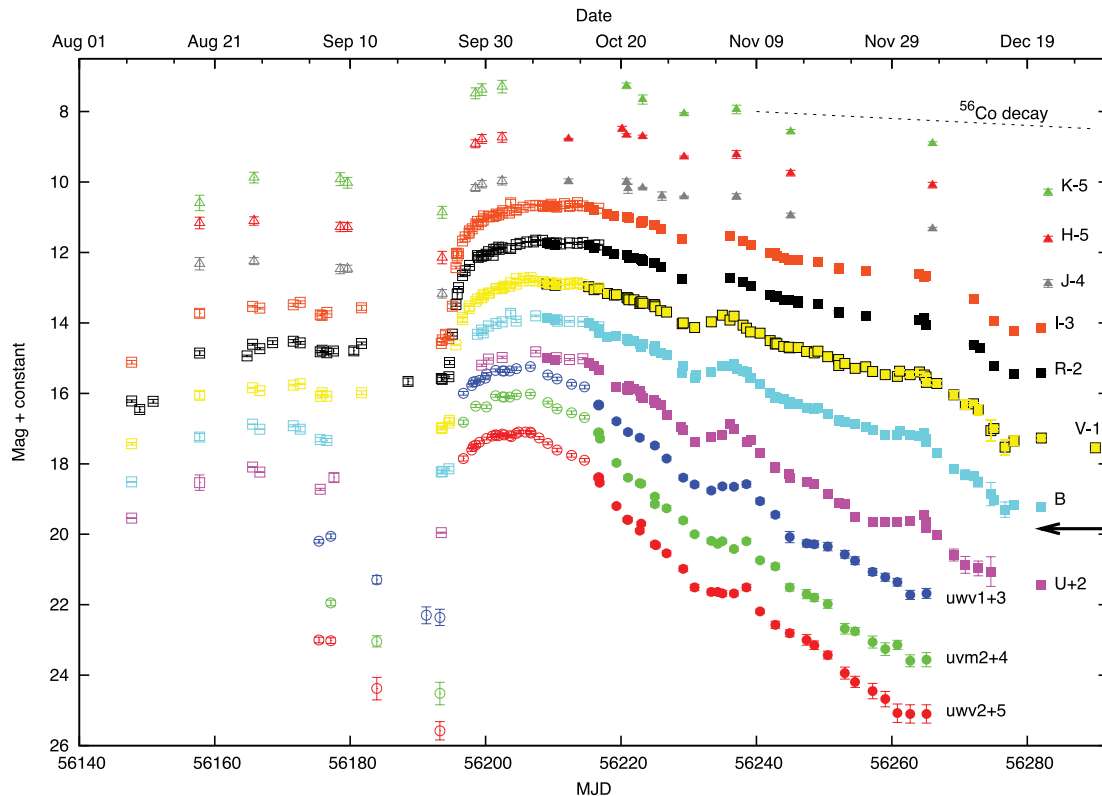

Figure 11. Optical (square points), UV (round points) and NIR (triangle points) photometry of SN 2009ip for the 2012a and 2012b events. The open points are taken from the data published by P13, while the filled points denote new data presented in this paper. We also include the *JHK* magnitudes reported for October 29 by Im (2012). Also indicated are the quiescent *F*606*W* (*R*) magnitude of the progenitor from Foley et al. (2011) (solid arrow, offset by −2 mag to match the *R*-band magnitudes of SN 2009ip) and the expected 0.98 mag per 100 d decline rate in *V* given by the radioactive decay of ^{56}Co (dashed line).
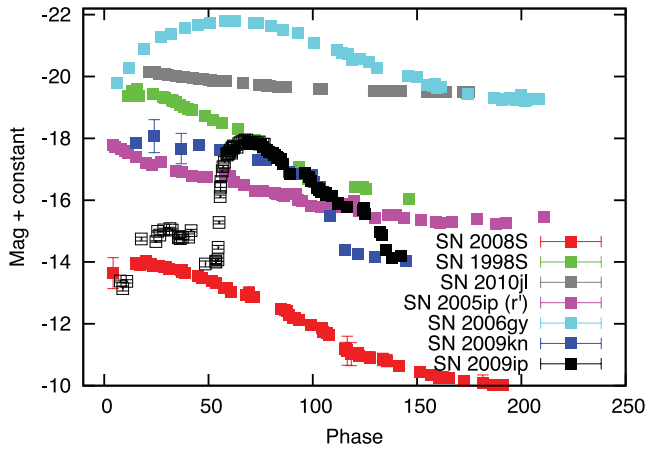
Figure 13. Comparison of the absolute *R*-band light curve of SN 2009ip with a selection of interacting transients (SN 2008S, $t_0 = 54\,485.5$, $A_R = 1.6$, $\mu = 28.7$, Botticella et al. 2009; SN 1998S, $t_0 = 50\,874.7$, $A_R = 0.56$, $\mu = 31.15$, Fassia et al. 2000; SN 2010jl, $t_{max} = 54\,887.5$, $A_R = 0.06$, $\mu = 33.44$, Zhang et al. 2012; SN 2005ip, $t_{disc} = 53\,679.2$, $A_R = 0.011$, $\mu = 32.71$, Stritzinger et al. 2012; SN 2006gy, $t_0 = 53\,976.0$, $A_R = 1.68$, $\mu = 34.32$, Smith et al. 2007; SN 2009kn, $t_0 = 55\,115.5$, $A_R = 0.25$, $\mu = 34.23$, Kankare et al. 2012). Light curves are plotted with respect to the explosion epoch (t_0), or where a good estimate of this is unavailable, to the discovery date (t_{disc}) or epoch of maximum light (t_{max}). Distances and extinctions are taken from the literature.

brightness. Unfortunately, the second bump coincides with the point at which SN 2009ip is too faint to observe in the UV with *Swift*, while the *R* and *I* bands are sparsely sampled to clearly identify the peak of the bump. The December bump lasts for a similar duration to the one in November – perhaps a week or less – and is followed by a continuing decline in the light curve afterwards. From around December 17 (MJD 562 78) the light curve appears to flatten until the last epoch on December 29.

In Fig. 13 we compare the *R*-band light curve of SN 2009ip over 2012 August–December to a sample of interacting transients taken from the literature. The peak magnitude of SN 2009ip, ~ -18, is comparable to that of SNe 2005ip and 2009kn, but much fainter than that of Type IIn SNe such as SN 2010jl and 1998S. SN 2009ip also has the most rapid decline from the peak of any objects in the sample.

The colour evolution of SN 2009ip is presented in Fig. 14. For the 2012a event, and up to the peak of the 2012b event, the colour in all optical bands is flat. As the SN fades from the peak of the 2012b event, the colour becomes redder in all bands as the photosphere cools. The colour evolution from photometry is in accord with that expected from the spectra, which shows a similar slope until peak. The $B - V$ colour shows a bump around the same time as the November 7 undulation in the light curve, which is to be expected given the time difference between the bump in different filters, as discussed in Section 4.2. A comparison to other interacting transients (SNe 1998S and 2009kn) shows a good match with SN 2009ip, with the only notable difference being a bluer $U - B$ colour for the latter compared to SN 2009kn. The NIR colours of SN 2009ip are shown in Fig. 15. As in the optical, we see a similar colour evolution to SNe 2009kn and 1998S. The evolution of SN 2009ip is consistent with a cooling blackbody, and shows no evidence for an NIR excess which would signal dust formation.

We constructed a bolometric light curve for SN 2009ip from our UV, optical and NIR photometry. The measured magnitudes were converted into fluxes at the effective wavelengths of the fil-
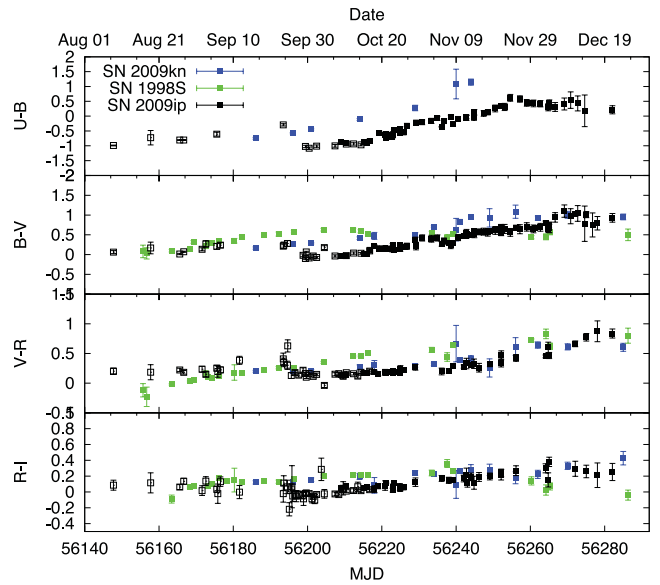

Figure 14. Optical colour curves for SN 2009ip during the 2012a and 2012b events. The open symbols are from P13, while the closed symbols are from this paper. SNe 2009kn and 1998S (Fassia et al. 2000; Kankare et al. 2012) are also shown; these objects have been shifted so that their explosion epoch is at MJD = 561 40.
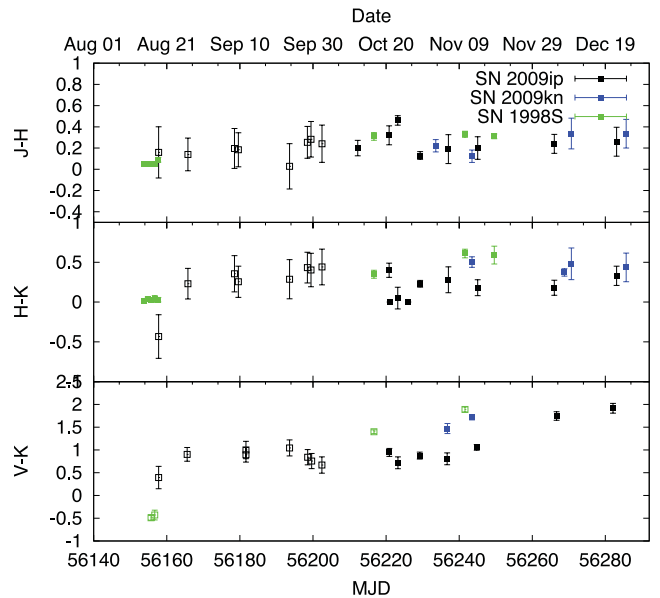

Figure 15. NIR colour curves for SN 2009ip during the 2012a and 2012b events. The open symbols are from P13, while the closed symbols are from this paper. We also include the *JHK* magnitudes reported for October 29 by Im (2012). SNe 2009kn and 1998S are also shown for comparison (Fassia et al. 2000; Kankare et al. 2012), and are shifted so that their explosion epoch would be at MJD = 561 40. All colour curves have been corrected for reddening.

ter used and corrected for extinction, before the resulting spectral energy distribution was integrated over the wavelengths covered with a linear interpolation, assuming zero flux beyond the limits of the integration. Fluxes were computed at epochs where there was an observation in *V*; where observations in other bands were not taken contemporaneously, their magnitudes were estimated by interpolating the light curves using low-order polynomials or were
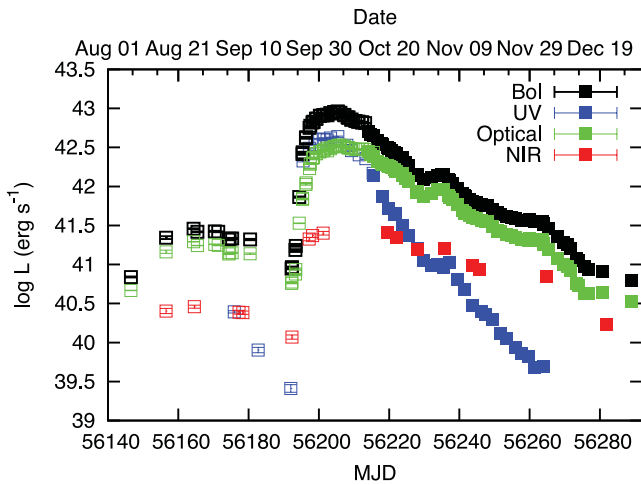
Figure 16. The *uvoir* bolometric light curve of SN 2009ip (black), together with the contributions of the optical, UV and NIR photometry.
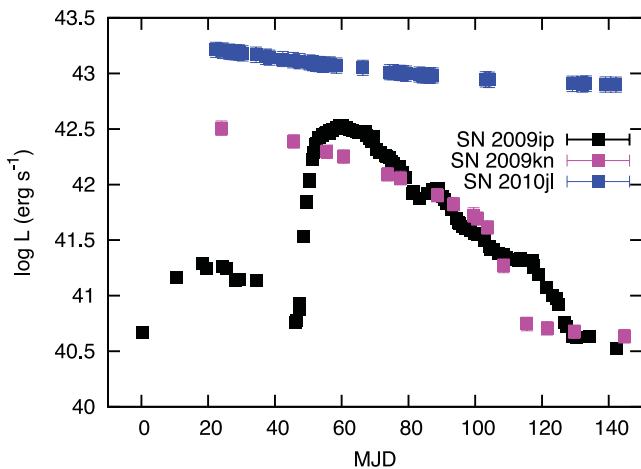

Figure 17. The pseudo-bolometric (*UBVRI*) light curve of SN 2009ip (black), together with two other well-observed Type IIn SNe: SN 2009kn (Kankare et al. 2012) and SN 2010jl (Zhang et al. 2012). The light curves of SNe 2009kn and 2010jl are relative to their explosion date, while that of SN 2009ip is relative to the start of the 2012a event.

extrapolated assuming constant colours. The bolometric flux at each epoch was converted to a luminosity given the adopted distance to SN 2009ip. The resulting bolometric light curve is shown in Fig. 16, and is compared with those of the interacting transients SNe 2009kn and 2010jl in Fig. 17. The bolometric light curve of the 2012a event is dominated by optical light. For the rising phase of the 2012b event however, the contribution to the light curve from the UV is larger than from optical wavelengths. The NIR contributes very little flux to the light curve of SN 2009ip for almost the entire duration of the 2012a and 2012b outbursts, amounting to only 20 per cent of the total at the time of our last epoch of NIR photometry.

4.2 The undulations in the light curve of SN 2009ip

The presence of bumps in the light curve of SN 2009ip is unusual (but not unprecedented, as they were also noted in the Type IIn SN 2005la; Pastorello et al. 2008). To reproduce these short bumps with the interaction of a few solar masses of ejecta (as might be ejected in a Type IIn SN) with the CSM may be difficult, as a massive SN ejecta should be more homogeneous (e.g. Gawryszczak

et al. 2010) and does not give rise to small-scale variations in the light curve. It is also possible that the bumps are periodic, although monitoring over a longer time-scale is needed to confirm this. In this case, the bumps could possibly be caused by spiral density structures resulting from a passage of a binary companion (e.g. Weiler et al. 1992; Maercker et al. 2012).

Another surprising aspect of the bumps is that they appear to peak first in the redder bands. Dust is unlikely to be the cause of the lag in the UV, as while it may cause the bump to be less pronounced at bluer wavelengths, there is no obvious reason why the peaks of the light curve in different filters would not coincide.

An alternative explanation for the shift in peak with wavelength is successive scattering by metal lines in the UV. The peak in *U* and the *Swift* UV filters is approximately 1–2 d after the peak in *BVRI*. To explain this delay with an additional travel time for UV photons implies that they cover a distance of 170–340 au *more* than the optical and NIR photons. For a characteristic radius of ∼40 au to the cool dense shell, this requires each photon undergoes multiple scattering events. It is also important that the photons (or at least a high percentage of them) scatter from the lines (which will give rise to re-emission at the same wavelength), rather than causing the atom to fluoresce (which would shift flux towards redder wavelengths) or undergo collisional de-excitation.

There is no marked change in the spectra of SN 2009ip around the time of the first bump. The [Ca II] begins to emerge at this epoch, which may indicate a lower density, but it is difficult to envisage a decrease in density causing a rise in luminosity.

4.3 Is there Ni in SN 2009ip?

The final epochs of photometry obtained for SN 2009ip before it disappeared behind the Sun appear to show a flattening in the redder bands. Given that the light curve displayed undulations prior to this (as discussed in Section 4.2), it is entirely possible that the apparent flattening is merely the start of a third bump in the light curve, rather than the beginning of any ^{56}Ni-powered tail phase. We note that the overall decline in the light curve from peak (4.5 mag over 80 d in *V*) is much faster than that expected from the decay of ^{56}Co (0.98 mag per hundred days).

From our final photometric point on December 29, we can estimate an upper limit to the mass of ^{56}Ni synthesized in SN 2009ip (assuming that it was indeed a genuine SN). We measure a bolometric luminosity of $\log(L) = 40.8$ erg s^{-1} for SN 2009ip on December 29. Using equation 2 of Hamuy (2003), and assuming that SN 2009ip exploded on 2012 August 1, we calculate a ^{56}Ni mass of <0.02 M$_\odot$. This is an upper limit to the mass of ^{56}Ni in SN 2009ip, as it is based on the earliest plausible date for an SN explosion (Mauerhan et al. 2013a). If the 2012a was not an SN, but rather the star exploded at the start of the 2012b event, then the ^{56}Ni mass must be less than 0.01M$_\odot$. Furthermore, Hamuy (2003) assumes that the sole energy source powering the luminosity of the tail is radioactive decay, whereas in the case of SN 2009ip there is at least some luminosity arising from interaction (as evidenced by the persistence of narrow emission lines until this epoch).

One caveat to this calculation is that the formation of dust can serve to mask the late-time luminosity of SNe at optical wavelengths, and cause their ^{56}Ni mass to be underestimated. However, in the case of SN 2009ip, we see no evidence for dust formation in either spectroscopy (no apparent blue shift of lines) or in photometry (no strong NIR excess). A second caveat is that we assume that γ-rays from the decay of ^{56}Co are fully trapped within the

ejecta. For the well-observed SN 1987A (Suntzeff & Bouchet 1990), approximately 2/3 of γ-rays were still trapped at 500 d post-explosion. The ratio of the trapping time-scale in SN 2009ip to that in SN 1987A will scale as $\left(M_{09ip}/M_{87A}\right)^{0.5}\left(v_{09ip}/v_{87A}\right)^{-1}$. If we assume that the velocities are roughly similar in the two events, and that the ejecta mass of SN 1987A was 12M$_\odot$, then this scaling implies that for γ-ray leakage to be significant at 100 or 150 d (depending on assumed explosion epoch), the ejecta mass in SN 2009ip should be less than 0.5 or 1.1 M$_\odot$, respectively. Such a small ejecta mass is much lower than that typically seen in SNe, and appears inconsistent with the core collapse of a massive star. Even with these caveats, the restrictive upper limit on the mass of any ^{56}Ni in SN 2009ip appears robust.

4.4 The energetics of SN 2009ip

Integrating under the *uvoir* bolometric light curves of the 2012a and 2012b events, we find an observed radiated energy of 7.8×10^{47} erg for the former and 1.8×10^{49} erg for the latter. In a normal CCSN, the radiated energy over the first one hundred days is typically comparable to that radiated in the 2012b event, $\sim 10^{49}$ erg.

While the large energy of the 2012b event is suggestive of a genuine SN explosion, with core collapse as the energy source, it is interesting to consider the possibility that the high luminosity is in fact completely due to the efficient conversion of kinetic energy from colliding ejecta. From the broad absorptions in the Balmer lines, we see material at velocities up to 12 000 km s^{-1}; however, we adopt 7500 as a more typical velocity for the bulk of the ejecta. If we assume 100 per cent efficiency in converting kinetic energy to radiation, then we only require 0.05 M$_\odot$ of material at 7500 km s^{-1} to give rise to the luminosity of the 2012b event.

To check whether the assumption of high efficiencies in the conversion of kinetic energy is correct, we apply the Rankine–Hugoniot conditions to the shock. For ejecta moving at v_{ej} hitting a reverse shock at v_{rs}, the efficiency ϵ in converting kinetic energy to luminosity is given by

$$\epsilon = \zeta \frac{v_{ej}^2 - (\eta v_{ej} + (1-\eta)v_{rs})^2}{v_{ej}^2}, \tag{1}$$

where ζ is the porosity (Area$_{clumps}$/Area$_{CSM}$) to account for clumpiness in the CSM, and η is the ratio of post- and pre-shock velocities in the rest frame of the shock. η depends on the equation of state of the gas, ranging between 1/4 and 1/7 for a perfect gas and a radiation-dominated gas, respectively. If we take the reverse shock to be moving at approximately the velocity of the photosphere derived from our blackbody modelling, 1200 km s^{-1}, and the ejecta to be moving at a conservative estimate of 7500 km s^{-1}, then we derive efficiencies of around 90 per cent. These efficiencies will be reduced by ζ, although even if 50 per cent of the CSM shell was clumps and 50 per cent was holes, then we would still have $\epsilon \sim 0.45$. In this case, we would still only require $\sim$0.1 M$_\odot$ of ejecta to power the interaction luminosity.

5 MODELLING THE CSM AROUND SN 2009IP

As a first attempt at understanding the physical conditions in SN 2009ip, we have constructed a spherically symmetric CSM model of SN 2009ip with a density profile R^{-2} as detailed in Appendix A. While the real structure of SN 2009ip is undoubtedly much more complex, with multidimensional effects and probably multiple shocked regions (Dwarkadas & Gruszko 2012), less com-
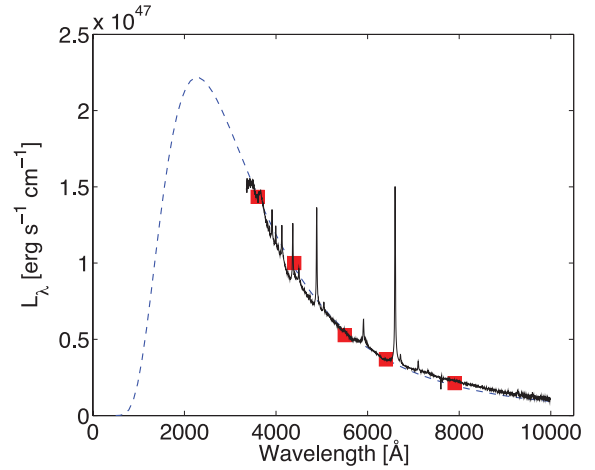
plex models can hopefully be used to derive order-of-magnitude results.

We perform a least-squares fit for blackbody radii and temperatures $[4\pi R_*^2 \pi B_\lambda(T_*) = L_\lambda]$ to the observed, dereddened, *UBVRI* photometry for selected epochs (typically the ones with full photometric coverage). The fit for the epoch we model in detail in Section 5 (2012 October 8) is shown in Fig. 18 as an example, while the time evolution of the derived radius and temperature is shown in Fig. 19. The radius at the start of the 2012b event derived from a blackbody fit is also consistent with the maximum radius derived from light travel time considerations using the high-cadence photometry presented by Prieto et al. (2013). The evolution observed over the 2012b event is quite similar to that seen in SN 1994W, which peaked at 15 000 K and declined to 7000 K over 70 d, but hotter than that of SN 2009kn, which only peaked at 10 000 K (Kankare et al. 2012). However, as the first spectra of SN 2009kn were obtained later than for SN 1994W, it is possible that the maximum temperature was in fact higher. Comparing to the radius evolution of SNe 1994W and 2009kn, we see that the initial photospheric radii of both these

Figure 18. The (dereddened) spectrum on 2012 October 8 (black, solid), together with (dereddened) photometry (red points) and blackbody fit to the photometry (blue, dashed). The derived temperature is 12 650 K.
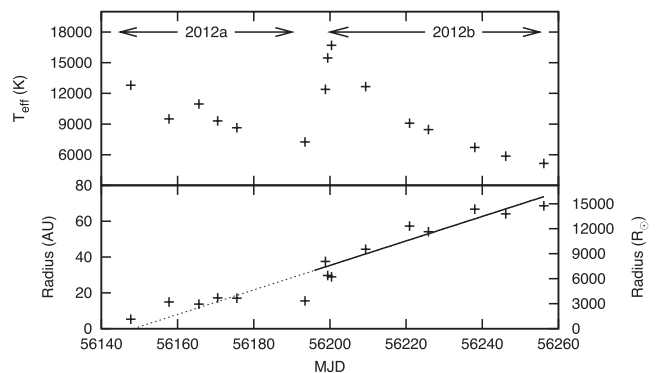
Figure 19. Upper panel: the temperature evolution of SN 2009ip as measured from blackbody fits to optical photometry at selected epochs. The approximate dates of the 2012a and 2012b events are indicated. Lower panel: the photospheric radius of SN 2009ip as determined from blackbody fits to optical photometry. The solid line shows a least-squares fit to the radii measured for the 2012b event only, while the dashed line denotes the extrapolation of that fit to the earlier 2012a event. The slope of the fit is 1200 km s^{-1}.

objects ($R \sim 8500\,R_\odot$) were larger than that of SN 2009ip during the 2012a event ($R \sim 3000\,R_\odot$), but that they expanded with similar velocities to the $1200\,\mathrm{km\,s^{-1}}$ observed in the 2012b event ($v_{\mathrm{SN1994W}} = 1000\,\mathrm{km\,s^{-1}}$, $v_{\mathrm{SN1994W}} = 1000\,\mathrm{km\,s^{-1}}$, $v_{\mathrm{SN2009kn}} = 600\,\mathrm{km\,s^{-1}}$).

We use the photospheric temperatures and radii derived as radiative boundary conditions for computing the ionization and excitation balance of hydrogen in the CSM as described in Appendix A. We do not solve for temperature, but assume $T = T_*$, which should be a reasonable approximation.

In particular, we investigate the first epoch after maximum light when we have an optical spectrum, MJD = 562 09 d, when $T_* \approx 12\,600\,\mathrm{K}$ and $R_* \approx 44$ au. The lack of any strong broad lines from the ejecta at this epoch, combined with the large photospheric radius, is possibly due to the formation of a cool dense shell at the interface between the outer ejecta and CSM, which becomes optically thick in the Paschen continuum for a few weeks if the CSM density is high enough (Chugai 2001). Outside this will be a region of shocked CSM, and outside the forward shock a region of unshocked CSM, radiating due to ionization by the photospheric radiation field (as well as from X-rays from the forward shock, which we however do not include here). Another possible explanation for the lack of broad absorptions is that the fast material is efficiently ionized by the emission from the shock region.

We explored the sensitivity of the model to having a region between the photosphere and the CSM, but do not find a significant difference.

For the inner parts of the CSM, the photospheric radiation field is strong enough that radiative processes are important not only for the ionization balance but also for the non-local thermodynamic equilibrium (NLTE) solutions to the excitation balance.

We may therefore not use standard recombination theory, which assumes that the external radiation field is negligible for the statistical equilibrium [as it is in normal H II regions where the dilution factor $(R/R_*)^2$ is large].

We explore models with different assumptions for the velocity gradient in the CSM (as discussed in Appendix A). Fig. 20 shows that a model with a zero velocity gradient (i.e. a constant velocity flow throughout the emitting region) is not successful in reproducing
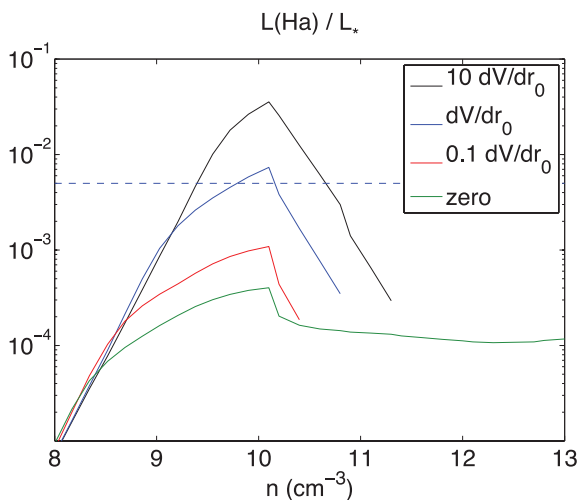

Figure 20. Ratio of Hα and photospheric luminosity, on 2012 October 8 (first spectrum after maximum light). The observed value (5×10^{-3}) is marked with a dashed line. The models with a velocity gradient are terminated at the density where the Sobolev limit is no longer reached (at high densities they behave as the model with zero gradient).

the observed strength of Hα.[8] This is a consequence of the efficient line trapping in a constant velocity flow; when the density becomes high enough to trap any significant fraction of the photospheric radiation ($n \gtrsim 10^9\,\mathrm{cm^{-3}}$), H$\alpha$ has such a high optical depth that $n = 3$ (the level creating Hα) becomes depopulated by collisions and photoionization rather than spontaneous decay.

Models with velocity gradients $\mathrm{d}V/\mathrm{d}r \gtrsim \mathrm{d}V/\mathrm{d}r_0$ ($\sim 1.4 \times 10^{-7}$, our estimated velocity gradient found by dividing the CSM velocity by the scale size of the region) produce more promising values of the Hα luminosity for densities $n \sim 10^9$–$10^{10}\,\mathrm{cm^{-3}}$. Turning to Figs 21(a) and (b), we see that these models also produce correct line ratios of $L(\mathrm{H}\alpha)/L(\mathrm{H}\beta) \approx 2$ and $L(\mathrm{H}\gamma)/L(\mathrm{H}\beta) \approx 0.45$. As Fig. 21(c) shows that Hα is marginally optically thick in these models, the reason for the damped Balmer decrement seems to be that Hα has an optical depth of a few, but Hβ is optically thin, a scenario discussed by Levesque et al. (2012).

Fig. 21(d) shows that all models predict electron scattering optical depths of order unity for densities between $n = 10^9$ and $10^{11}\,\mathrm{cm^{-3}}$. Since the Balmer lines show distinct broad wings that likely arise due to electron scattering with optical depth of the order of a few (Chugai 2001; Chugai et al. 2004; Dessart et al. 2009; Smith et al. 2010b), this further strengthens the idea that the CSM density lies in this interval.

As made clear by the previous figures, the high density $n \gtrsim 10^{13}\,\mathrm{cm^{-3}}$ proposed by Levesque as one possibility for the low Balmer decrement is not successful in reproducing the observables. At these high densities, the Balmer lines have high optical depth for any reasonable assumption about the velocity field, and as the level populations also approach local thermodynamic equilibrium, the line ratios approach their blackbody values. As an example, the Hγ/Hβ ratio goes towards 1.3 at high densities (and $T = 12\,000$ K), whereas the observed value is ~ 0.45, as reproduced by the NLTE models around $n = 10^9$–$10^{10}\,\mathrm{cm^{-3}}$. A high-density model would need $T \sim 2500$ K to reproduce the Hγ/Hβ ratio, but at that temperature the Balmer decrement has a value of 4.8, much too high. The other model result that clearly rules out an $n \gtrsim 10^{13}\,\mathrm{cm^{-3}}$ scenario is that that the electron scattering optical depth would be much smaller than unity.

The number density for a constant mass-loss rate at a radius r is

$$n(r) = \frac{\dot{M}}{\bar{A}m_p 4\pi r^2 v(r)}$$

$$= 5 \times 10^{10}\,\mathrm{cm^{-3}} \left(\frac{\dot{M}}{1\,\mathrm{M_\odot\,yr^{-1}}}\right)\left(\frac{r}{40\,\mathrm{au}}\right)^{-2}\left(\frac{V}{10^3\,\mathrm{km\,s^{-1}}}\right)^{-1},$$
$$(2)$$

where $\dot{M}$ is the mass-loss rate, $\bar{A}$ is the mean atomic weight (1.6 for a normal H/He mix), m_p is the proton mass and $v(r)$ is the wind velocity. The derived density of $n \sim 10^9$–10^{10} therefore suggests as a mass-loss rate of $\dot{M} \sim 0.01$–$0.1\mathrm{M_\odot\,yr^{-1}}$. We caution, however, that this is likely only correct to an order of magnitude, due to the uncertain assumption of a constant mass-loss rate.

Using more sophisticated modelling, Dessart et al. (2009) find a similar Balmer decrement of ~ 2 for SN 1994W from a model with a density of 10^9–$10^{10}\,\mathrm{cm^{-3}}$ and with a velocity of $\sim 800\,\mathrm{km\,s^{-1}}$.

---

[8] The observed value was obtained by measuring the relative amount of flux in the line compared to the total flux in the spectrum (3300–10 000 A), plus estimated fluxes outside the spectral range from the blackbody fit. This gives a fraction of 5×10^{-3}. Assuming no flux outside the spectrum, the value is 0.012.
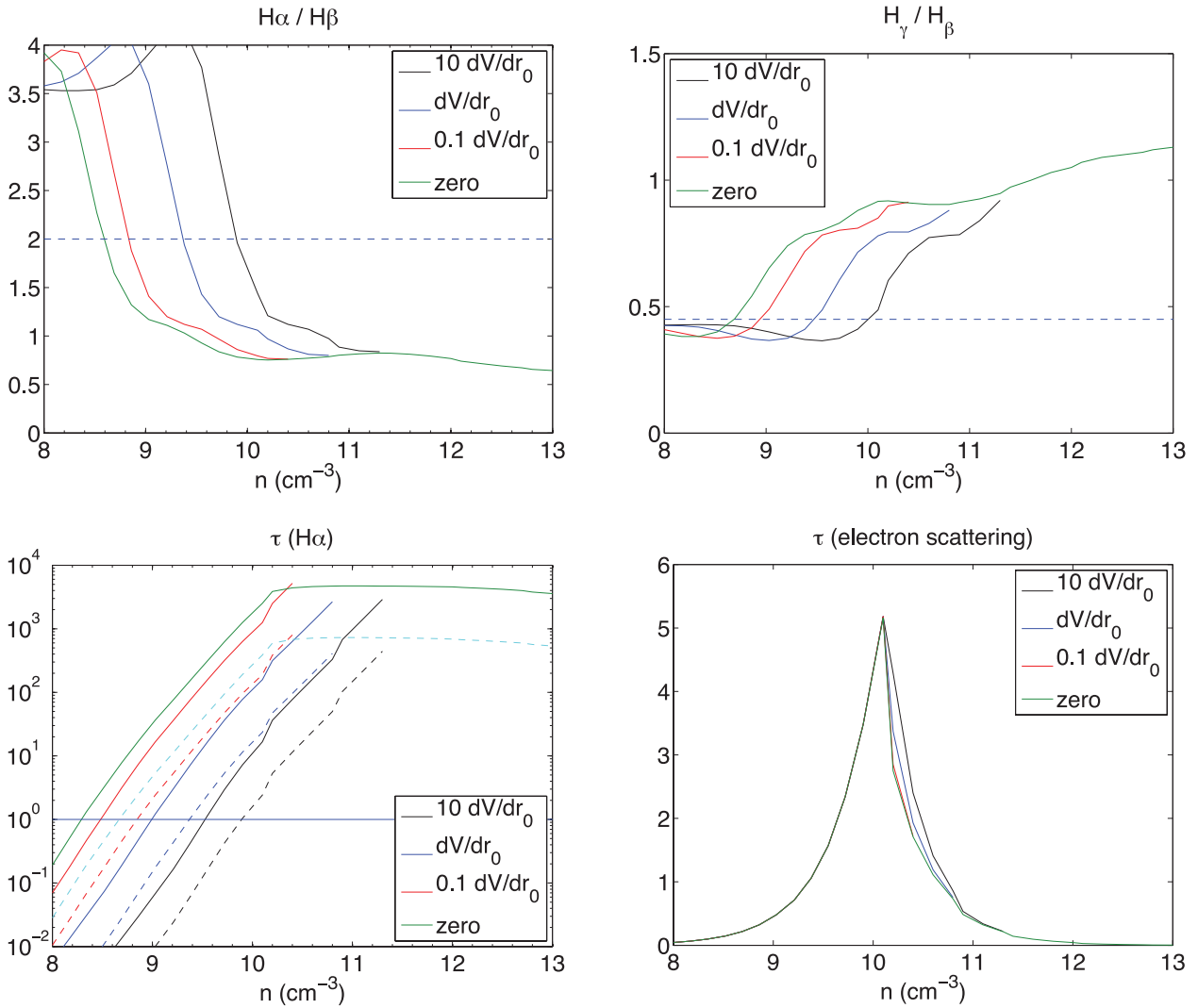
Figure 21. Results from our modelling as described in Section 5. (a) Hα/Hβ ratios as a function of density in our models for the CSM lines around the maximum of the 2012b event. The observed value is indicated with a dashed line. (b) Same as Fig. 21(a), but for the Hγ/Hβ ratio. (c) Model Hα (solid) and Hβ (dashed) optical depths around the peak of the 2012b event. (d) Electron scattering optical depths in our models for the CSM lines around the peak of the 2012b event.

Chugai et al. (2004) also require a similar density in order to reproduce the electron scattering wings. That these values are in close agreement with our simpler calculations lends credence to our approach.

6 ANALYSIS

There are three questions which are key to understanding SN 2009ip. First, what is the significance of the surprisingly remote location of SN 200ip; secondly, was either of the 2012a/b events an SN explosion or a mega-outburst of an impostor; and thirdly, what powers the luminosity of the 2012a/b events? As these questions are linked, we will address them in turn.

6.1 The lonely fate of SN 2009ip

One of the most striking features of SN 2009ip is its isolated location, as illustrated in Fig. 22. SN 2009ip is at a projected distance of ∼0.75 arcmin from the centre of NGC 7259, placing it at a de-projected physical distance of 4.3 kpc. To measure the radial extent

of the galaxy, we took the deepest *R*-band images of SN 2009ip taken with EFOSC2 under 1 arcsec seeing or better (from 2011 June 23), and stacked them to create a deep 1200 s exposure. No faint spiral arm or other obvious structure can be seen at the SN location; in fact, the nearest extended source to SN 2009ip in NGC 7259 is ∼10 arcsec distant. We measure a surface brightness at the SN location of $R = 25$ mag arcsec^2. The radial extent of NGC 7259 has been measured at 0.6–0.78 arcmin for surface brightness of 25 and 27 mag arcsec^2, respectively (as listed in the NASA/IPAC Extragalactic Database, from Lauberts & Valentijn 1989). Hence, although there is little star formation in the vicinity of SN 2009ip, it appears to reside within the optical disc of the galaxy.

After masking the nearby galaxy 2MASXi J2223042−285647 in our deep image, we performed aperture photometry on NGC 7259 using circular apertures between 5 and 250 pixels (i.e. to a maximum radius of 1 arcmin). The sky background was measured in a blank region of the image several arcminutes distant from NGC 7259 to avoid any unintended contamination. We plot the enclosed flux from NGC 7259 as a function of radius in Fig. 23 in a similar fashion to Anderson & James (2009). The fraction of *R*-band light within the
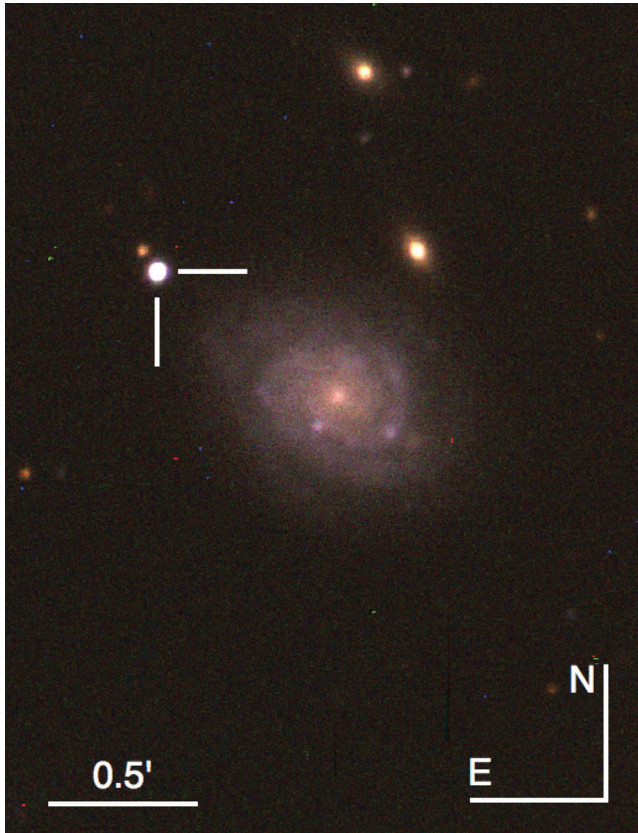
Figure 22. *BVr* colour composite of SN 2009ip (marked with cross hairs) and NGC 7259 obtained with the Liverpool Telescope + RATCAM on 2012 November 13. Scale and orientation are as indicated. The 0.5 arcmin scale bar corresponds to a physical distance of approximately 3 kpc at the distance of NGC 7259.
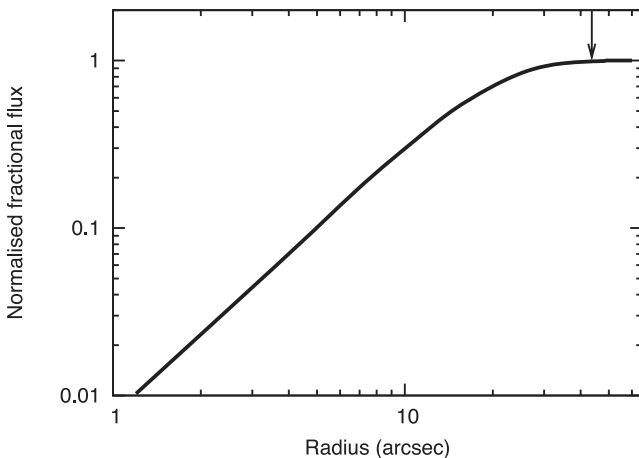

Figure 23. Enclosed *R* flux from NGC 7259 as a function of radius, normalized to total flux. The arrow indicates the position of SN 2009ip, which lies outside the detectable extent of the galaxy.

position of SN 2009ip, F_{rR}, is $\simeq 1$. Anderson & James found that the mean F_{rR} for Type IIn SNe and SN impostors was slightly larger than for Type IIP SNe, and that there was a deficit of both impostors and Type IIn SNe in the central regions of galaxies. While SN 2009ip is in agreement with this trend, it is an extreme example, and indeed has a larger value of F_{rR} than any of the interacting transients in their sample. This is also in accord with Anderson et al. (2012), who

found that SN impostors and Type IIn SNe are the least correlated with ongoing star formation as measured from Hα and UV imaging. It is worth noting, however, that the 'SN impostor' category of Anderson et al. (2012) is extremely heterogeneous and contains quite dissimilar transients (for example SN 2008S, Botticella et al. 2009 and SN 2002kg, Maund et al. 2006; Weis & Bomans 2005). Nonetheless, the location of SN 2009ip is quite unique among both Type IIn SNe and SN impostors. Anderson et al. (2012) have used the argument that the lack of correlation of Type IIn SNe with Hα emission implies that they have lower mass progenitors than the bulk of the CCSN population. While SN 2009ip is certainly isolated from any strongly star-forming regions, it has (without doubt) a high-mass progenitor star.

The *HST*+Wide Field Planetary Camera 2 *F606W* images presented by Foley et al. (2011) are also of use for constraining the environment of SN 2009ip. Using HSTPHOT (Dolphin 2000), we detect only a single source[9] within a 4 arcsec radius of SN 2009ip. We calculate a limiting magnitude of $F606W > 25$ mag, implying that there is only a single source with an *R* magnitude brighter than -6.6 within a 500 pc radius of SN 2009ip.

The apparently isolated position of SN 2009ip is of interest for two reasons. First, as an LBV with a ZAMS mass of $\sim$50–60 M$_\odot$, the progenitor of SN 2009ip could be an example of isolated star formation. While there are examples of isolated massive stars in the Large Magellanic Cloud (for example VFTS 682; Bestenlehner et al. 2011), these are still within a few tens of parsec of a massive star-forming region, and in the case of VFTS 682 have been suggested to have been dynamically ejected from a young cluster with a top-heavy initial mass function (Banerjee & Kroupa 2012). For SN 2009ip, there is no obvious nearby cluster, even with a runaway velocity of 50 km s^{-1}, permitting it to cover a distance of 500 pc in 10^7 years. Secondly, the extreme radial location also points towards a sub-solar metallicity. Applying the metallicity gradient of Boissier & Prantzos (2009) to the position of SN 2009ip, and estimating the characteristic metallicity of NGC 7259 from its *B*-band magnitude, we find a local metallicity of $12+\log(O/H) = 8.5$ dex. This value is significantly lower than the locus of SN metallicites derived by Boissier & Prantzos using the same technique on a sample of SN host galaxies. Unfortunately, there is no nearby H II region where we could obtain a spectroscopic estimate of the metallicity, while the auroral [O II] and [O III] lines are not detected in our spectra precluding a direct measurement of the electron temperature and metallicity.

6.2 Has SN 2009ip exploded as an SN?

Ultimately, the most definitive proof that a star has exploded as a CCSN is the disappearance of its progenitor in late-time images taken after the explosion has faded. While it should be possible to eventually test this for SN 2009ip, at the time of the final photometry obtained of SN 2009ip at the end of December, the transient was still $\sim$4.5 mag brighter than the progenitor detected by Foley et al. (2011). If the 2012b event continues its decline rate from a maximum of $\sim$3.5 mag in 70 d, then by the time SN 2009ip reappears in 2013 mid-April, we may expect it to be fainter than the magnitude of the progenitor if it was a genuine SN. However, an ongoing

[9] We are excluding here the foreground star ($R \sim 18.4$) to the NE of SN 2009ip.

interaction may slow this decline, and lead to a source remaining at the site of SN 2009ip which is brighter than the progenitor magnitude for an extended period. Similarly, we cannot rule out the possibility that the progenitor of SN 2009ip was in a binary system, in which case a surviving companion star could remain. Spectroscopy at late epochs could help determine the nature of any surviving source, and at the apparent magnitude of the quiescent progenitor, it would be feasible with an 8 m class telescope.

Another critical piece of evidence for an SN explosion is the detection of nucleosynthesized material in the ejecta. This may be either explosively produced isotopes (e.g. ^{56}Ni) or elements synthesized during the later stages of stellar evolution (e.g. ^{16}O). In SN 2009ip we do not see any evidence for freshly synthesized material; all the lines present in the December 20 spectra were also present in 2009 September. We also see none of the usual lines which are typically seen in the nebular spectra of CCSNe such as [O I] 6300, 6364 Å, Mg I] 4571 Å and Mg I 1.5 μm. Against this, however, we must note that many Type IIn SNe do not show these lines until quite late phases, due to the low gas densities of $\sim 10^9$ cm^{-3} required. While for SN 1998S, the [O I] 6300 Å line emerged at +112 d after explosion (Liu et al. 2000), in other cases such as SN 1998Z (Turatto et al. 1993) or SN 2006jc (Stritzinger et al. 2012), an [O I] 6300 Å line was not visible up to at least +1000 d post-explosion.

Another signature of a CCSN is the presence of a radioactively powered tail phase, which at late times follows the decay rate of ^{56}Co. From our last photometric point, we set a limit of <0.02 M$_\odot$ of Ni in SN 2009ip. Such a low ejected Ni mass is difficult to reconcile with the core collapse of a very massive star, although a similarly low value of $\lesssim 0.023$ M$_\odot$ was set for SN 2009kn (Kankare et al. 2012), albeit with the caveat that the tail may not be Ni-powered. Umeda & Nomoto (2008) find that models with a ZAMS mass of 60–80 M$_\odot$ produce between 0.8 and 7.9 M$_\odot$ of Ni, depending on explosion energy. The low upper limit to the ejected Ni mass could be explained if much of the Ni did not escape, but rather underwent fallback on to the compact remnant. Such a scenario was proposed for SN 1997D (Turatto et al. 1998), although in the case of fallback the ejecta velocities are expected to be closer to 10^3 than 10^4 km s^{-1}.

We note that a low ejected Ni mass was also derived for the Type IIn SN 1994W (Sollerman et al. 1998). In this case, Chugai et al. (2004) claimed that the transient arose from the interaction of an SN with the hydrogen envelope of the star, which had been ejected 1.5 years prior. Chugai et al. proposed that the ejection of the envelope could be due to a Ne burning flash in the O–Ne–Mg core of an 11 M$_\odot$ star, while the low progenitor mass would also account for the small ejected Ni mass. The explosion of a super asymptotic giant branch star was also claimed for SN 2011ht by Mauerhan et al. (2013b), and suggested as a possibility by Kankare et al. (2012) for SN 2009kn. In the case of SN 2009ip, however, the massive progenitor is clearly inconsistent with such a scenario. An alternative model for SN 1994W was proposed by Dessart et al. (2009), who suggested that the collision of two ejected shells with an efficient conversion of kinetic energy to luminosity could also power the transient. In the colliding shells model, the progenitor star is not necessarily destroyed, although the lack of pre-explosion imaging coupled with its crowded environment makes this difficult to test for SN 1994W with deep, late-time imaging.

Less compelling indicators of a CCSN include high velocities and luminosities. In the case of the former, the observation by P13 of material at velocities of $\sim 10^4$ km s^{-1} in 2011, long before the start of the 2012a and 2012b events, suggests that the material can be accelerated to high velocities *without* a core-collapse explosion. The

bright absolute magnitude of SN 2009ip ($V = -17.7$) is certainly suggestive of core collapse; however, as we have shown in Section 4.4 the kinetic energy of a relatively small amount of material at the velocities observed can power the light curve. Furthermore, some of the most luminous SNe known have been suggested to arise from outbursts which do not (at least immediately) destroy the progenitor star (Woosley, Blinnikov & Heger 2007).

We compare the velocities of SN 2009ip in 2011 and 2012 in Fig. 24. The maximum velocity of Hα, as defined by the blue edge of the broad absorption, was ~ 1500 km s^{-1} higher in the 2012b event than in 2011. The He I/Na D blend at 5876–5896 Å shows higher velocities than Hα in 2012, and is markedly stronger than the broad absorption which we tentatively identify in the 2011 spectrum. In fact, the blue edge of the He I lines on November 20 lies at least at 17 000 km s^{-1}, while there is possibly some material at even higher velocities.

The biggest difference between the broad features seen in 2011 and those seen in 2012 is that the former were observed solely in absorption, while the latter were also seen in emission. In Fig. 1, the clearest broad emission is associated with Hα, He I and Ca. While Hα has a broad emission component of FWHM 8500 km s^{-1}, this value is less certain than for other lines due to its multicomponent nature. For the isolated He line at 7065 Å and the Ca NIR triplet, we measure velocities of ~ 3000 km s^{-1} from the FWHM of the lines. The presence of broad emission lines in 2012 implies that more material is moving at high velocities than in 2011. If the 2012a and 2012b outbursts of SN 2009ip are eruptions from an SN impostor, then they represent the highest velocities seen to date in such an event.

From the available evidence – and remaining mindful of the truism that 'absence of evidence is not evidence of absence' – we suggest that thus far there is no evidence that SN 2009ip did indeed undergo core collapse to produce either the 2012a or 2012b events.

6.3 What powers the luminosity of the 2012a and 2012b events?

Any scenario for SN 2009ip needs to explain the following key characteristics.

(i) An intrinsically luminous, a most likely very massive progenitor star, probably with a low metallicity.

(ii) Multiple eruptions over at least a 3 yr period, which eject material at velocities of up to 10^4 km s^{-1}.

(iii) A brief, 40 d eruption.

(iv) A subsequent more luminous eruption, with a fast rise time, which decays rapidly from peak.

(v) An ejected ^{56}Ni mass <0.02 M$_\odot$.

(vi) No observed synthesized material, either from explosive nucleosynthesis or late-stage stellar evolution.

There have been several suggestions as to the energy and nature of the 2012a and 2012b events. Mauerhan et al. (2013a) argued that the 2012a event was the explosion of SN 2009ip as a weak CCSN with a low ejected Ni mass, while the 2012b event was caused by the ejecta hitting the CSM. P13 further suggested that if SN 2009ip was indeed a genuine SN, then the 2012b event may be the explosion of SN 2009ip, while the 2012a event was an outburst. However, P13 also advanced an alternative scenario that SN 2009ip has not exploded as an SN, but rather that the light curve and spectra could be explained by the collision of two massive shells of material ejected by the progenitor (Dessart et al. 2009). Such an eruption could be powered by the pulsational pair instability
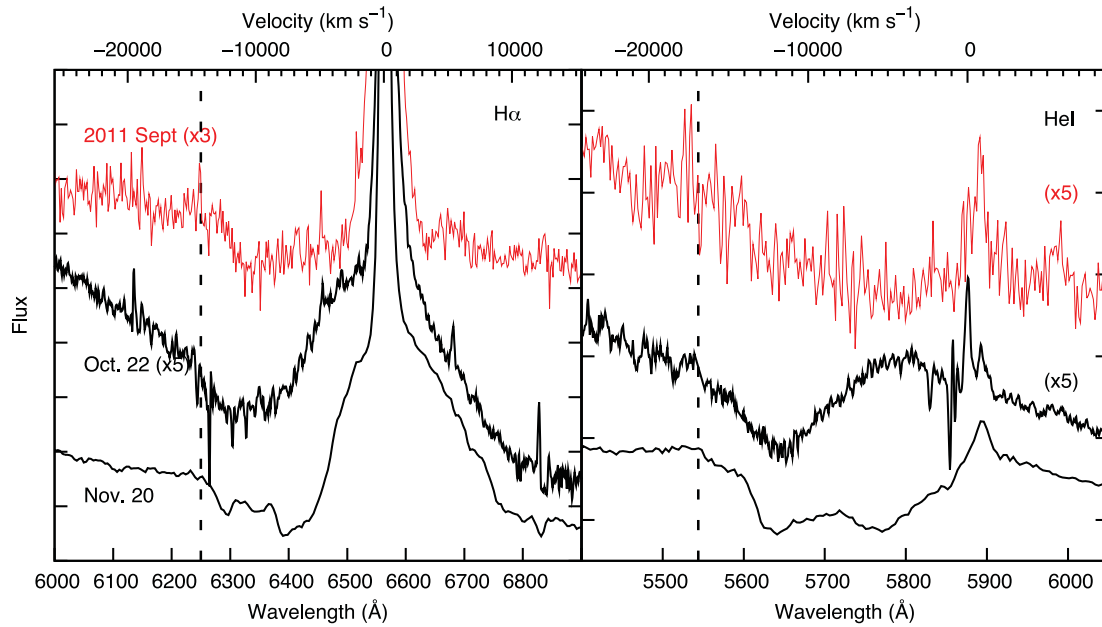
Figure 24. Detail of the high-velocity absorption associated with Hα (left-hand panel) and He I/Na D (right-hand panel) in 2012 October and November, as compared to that seen on 2011 September 24 by P13 (indicated in red). The blue edge of the absorption in the November 20 spectrum is marked with a dashed line; this was found to lie at $14\,250\,\mathrm{km\,s^{-1}}$ for Hα and $16\,900\,\mathrm{km\,s^{-1}}$ for the He I/Na D blend.

(Woosley et al. 2007). A final model for SN 2009ip was proposed by Soker & Kashi (2013), who favoured a merger of a massive LBV with a binary companion, in a 'mergerburst' model. Soker & Kashi draw comparison to the enigmatic transient V838 Mon, for which a similar scenario was proposed.

Soker & Kashi (2013) predicted that the light curve of SN 2009ip would decline from the peak of the 2012b event, with no subsequent major outbursts. Soker & Kashi also predicted a relatively small ejecta mass ($1-3\,\mathrm{M_\odot}$), most of which is moving at less than $5000\,\mathrm{km\,s^{-1}}$. This is in broad agreement with what we observe, although the real test of this model – namely the emergence of a surviving hot giant star – will have to wait several years. In this scenario, some of the previous outbursts of SN 2009ip could have been triggered by close approaches at periastron on orbits before the final merger, while others may be due to the intrinsic variability and eruptions associated with an unstable $\sim 60\,\mathrm{M_\odot}$ star.

As discussed in Section 6.2, while a weak CCSN explosion in the 2012a event cannot be entirely ruled out, we see no conclusive evidence in favour of it. Furthermore, while a weak explosion could explain the low ^{56}Ni mass, we would not expect to observe the high ejecta velocities seen. If the 2012b event was the SN, then the upper limit to the ^{56}Ni mass is even more restrictive. Whether an $\sim 60\,\mathrm{M_\odot}$ star can explode, suffer sufficient fallback to hide almost all its Ni, but still retain a strong enough explosion to drive the ejecta outwards at upwards of $10^4\,\mathrm{km\,s^{-1}}$ remains to be seen.

In the canonical model for the Type IIn SN, the luminosity is powered by an interaction between ejecta and the CSM. At the start of the 2012b event, the radius of the photosphere is around 30 au, and is expanding with a velocity of $1200\,\mathrm{km\,s^{-1}}$, as can be seen in Fig. 19. If the observed photosphere is formed at the cool dense shell, then any ejecta moving with a velocity of $>1000\,\mathrm{km\,s^{-1}}$ should reach this over the time-scales of the 2012b event. Any such ejecta will pass through the shocks, being decelerated and heated in the process. The fact that ejecta with velocities close to $10^4\,\mathrm{km\,s^{-1}}$ is still observed in our last spectra indicates that either the photosphere is not at the interaction region or the cool dense shell/interaction

region is clumpy, and that some of the fast ejecta can pass through it unhindered. The latter scenario could also help explain why even at the peak of the 2012b event there are weak broad absorptions. Such clumpiness is almost a certainty, given likely instabilities associated with the multiple shocks passing through the CSM due to past explosive events.

An alternative arrangement to explain the simultaneous presence of high-velocity absorption and interaction-dominated line profiles could be a disc or torus-like geometry, as suggested by Levesque et al. (2012). In such a scenario, most of the CSM lies in a disc, the polar axis of which is inclined relative to our line of sight. A fraction of the fast ejecta will impact the disc and give rise to the interaction, depending on the thickness of the disc and the precise emitting geometry.

The pulsational pair instability models of Woosley et al. (2007) and Chatzopoulos & Wheeler (2012) could reproduce well the observed characteristics of SN 2009ip, and that the high luminosity seen during the 2012b event is probably powered by colliding shells. The 2012a event could also be powered by interaction; alternatively it could be simply due to the internal energy released during an outburst. Either way, this prediction can be tested by observing the surviving progenitor star (or finding it has disappeared) once SN 2009ip emerges from behind the Sun in 2013 April. Accurate measurements of the metallicity at the site of SN 2009ip would also be of interest, given the expectation that pulsational pair instability eruptions should only occur at low metallicity.

In the Woosley et al. (2007) models of pulsational pair instability, the time-scale from the initial outburst to the final death of the star is around 15 yr. This is somewhat longer than the O burning time-scale of ~ 1 yr for a massive star (Woosley et al. 2002), possibly due to the additional time required for the star to relax back to its normal state after the first outburst. Still, if the pulsational pair instability is driving the recent mass-loss of SN 2009ip, then one may expect the star to explode as a genuine SN in the next few years. If SN 2009ip continues to erupt over a period much longer than a decade, then the pulsational pair instability can probably be discounted in the case

of SN 2009ip. It is also entirely possible that another mechanism, which could occur at earlier burning stages, has ejected a significant amount of material from SN 2009ip. The gravity wave-mediated instability proposed by Quataert & Shiode (2012) could possibly even occur during the C burning stage, in which case the ejection of several $M_\odot$ of material could occur $\sim10^3$ years prior to the exhaustion of a star's nuclear fuel.

The previous outbursts of SN 2009ip (dating back to its discovery in 2009 August) may also help constrain the true nature of SN 2009ip. If the 2012a and 2012b outbursts are not a core-collapse SN, then it is not unreasonable to expect the mechanism which powers them to have also powered the prior outbursts. Many questions remain about the pulsational pair instability which require detailed modelling beyond the scope of this paper. Most relevant to SN 2009ip, are whether pulsational pair instability can produce multiple weak eruptions, and whether the velocities can be higher, and ejected masses lower, than in the models presented by Woosley et al. (2007). The velocities in the Woosley et al. model were lower than those seen for the fastest material in SN 2009ip ($\sim4000\,\mathrm{km\,s^{-1}}$ in the former, compared to $\gtrsim10\,000\,\mathrm{km\,s^{-1}}$ in the latter), although only a single model was presented in this paper, and it is hence unclear what diversity can be found in the entire parameter space of the pulsational pair instability.

7 CONCLUSIONS

We have presented intensive UV, optical and NIR spectroscopy and photometry of the interacting transient SN 2009ip. The transient was intrinsically luminous at the peak of the 2012b event, but over the following weeks faded much more rapidly than is typically seen in CCSNe. From our photometry we have set a robust upper limit of $<0.02\,M_\odot$ to the mass of any ^{56}Ni synthesized in SN 2009ip. This limit can be considered secure with respect to both γ-ray leakage and dust formation. Spectroscopically, the transient shows a blue continuum with narrow emission lines from H and He, before developing strong broad absorption and emission in both H and He, along with Na and Ca. At no point do we see the nebular emission from synthesized material which is the hallmark of late-stage evolution in CCSNe.

From our modelling of the CSM, we find that densities of 10^9–10^{10} are sufficient to explain the narrow Balmer lines and the observed Balmer decrement. We also find that a velocity gradient is required in the CSM to reproduce the Hα to continuum ratio; such a gradient implies that the mass-loss is eruptive rather than a steady wind.

We see no evidence for core collapse in our data set, and in particular we do not observe the appearance of nebular emission lines or detect a radioactive tail. We suggest that the properties of SN 2009ip can be explained with the efficient conversion of kinetic energy to optical luminosity via colliding shells, possibly resulting from a pair-instability-driven outburst.

A final question posed by SN 2009ip – if it is indeed not a core-collapse SN – is whether other interacting transients have been similarly misclassified. Dessart et al. (2009) suggested that SN 1994W was not a CCSN, while the possibility was also raised by Kankare et al. (2012) for SN 2009kn. If the progenitor of SN 2009ip is seen to survive this latest eruption, it will confirm that a high peak luminosity and the detection of high-velocity ejecta cannot be regarded as definitive proof of core collapse in interacting transients. Of course, if such transients are powered by the pulsational pair instability, then it is likely that we will see recurrent outbursts on time-scales of years. SN 1994W is now nearly two decades after discovery,

with no detected subsequent outbursts, and so the pulsational pair instability seems less likely in this case. We stress, however, that the pulsational pair instability is not the only theorized mechanism for ejecting material from a star, and that it is still possible that SN 1994W was powered by colliding shells, which were ejected by another process.

REFERENCES

Aldering G. et al., 2006, ApJ, 650, 510
Anderson J. P., James P. A., 2009, MNRAS, 399, 559

Anderson H., Ballance C. P., Badnell N. R., Summers H. P., 2000, J. Phys. B: At. Mol. Phys., 33, 1255

Anderson J. P., Habergham S. M., James P. A., Hamuy M., 2012, MNRAS, 424, 1372

Banerjee S., Kroupa P., 2012, A&A, 547, A23

Bestenlehner J. M. et al., 2011, A&A, 530, L14

Boissier S., Prantzos N., 2009, A&A, 503, 137

Botticella M. T. et al., 2009, MNRAS, 398, 1041

Brocklehurst M., 1971, MNRAS, 153, 471

Capriotti E. R., 1965, ApJ, 142, 1101

Castor J. I., 1970, MNRAS, 149, 111

Chatzopoulos E., Wheeler J. C., 2012, ApJ, 760, 154

Chevalier R. A., Fransson C., 1994, ApJ, 420, 268

Chevalier R. A., Blondin J. M., Emmering R. T., 1992, ApJ, 392, 118

Chugai N. N., 2001, MNRAS, 326, 1448

Chugai N. N. et al., 2004, MNRAS, 352, 1213

Dessart L., Hillier D. J., Gezari S., Basa S., Matheson T., 2009, MNRAS, 394, 21

Dolphin A. E., 2000, PASP, 112, 1383

Dopita M., Hart J., McGregor P., Oates P., Bloxham G., Jones D., 2007, Ap&SS, 310, 255

Dopita M. et al., 2010, Ap&SS, 327, 245

Drake S. A., Ulrich R. K., 1980, ApJS, 42, 351

Drake A. J. et al., 2012, Astron. Telegram, 4334, 1

Dwarkadas V. V., Gruszko J., 2012, MNRAS, 419, 1515

Elitzur M., 1982, Rev. Mod. Phys., 54, 1225

Fassia A. et al., 2000, MNRAS, 318, 1093

Fassia A. et al., 2001, MNRAS, 325, 907

Fesen R. A., Hurford A. P., Matonick D. M., 1995, AJ, 109, 2608

Fesen R. A. et al., 1999, AJ, 117, 725

Foley R. J., Smith N., Ganeshalingam M., Li W., Chornock R., Filippenko A. V., 2007, ApJ, 657, L105

Foley R. J., Berger E., Fox O., Levesque E. M., Challis P. J., Ivans I. I., Rhoads J. E., Soderberg A. M., 2011, ApJ, 732, 32

Fox O. et al., 2009, ApJ, 691, 650

Gal-Yam A., Leonard D. C., 2009, Nat, 458, 865

Gal-Yam A. et al., 2007, ApJ, 656, 372

Gawryszczak A., Guzman J., Plewa T., Kifonidis K., 2010, A&A, 521, A38

Hamuy M., 2003, ApJ, 582, 905

Humphreys R. M., Davidson K., 1994, PASP, 106, 1025

Humphreys R. M., Davidson K., Jones T. J., Pogge R. W., Grammer S. H., Prieto J. L., Pritchard T. A., 2012, ApJ, 760, 93

Im M., 2012, Astron. Telegram, 4532, 1

Inserra C. et al., 2012, A&A, preprint (arXiv:1210.1411)

Jeffery D. J., Branch D., 1990, Supernovae, Jerusalem Winter School for Theoretical Physics. World Scientific Press, Singapore, p. 149

Johnson L. C., 1972, ApJ, 174, 227

Kankare E. et al., 2012, MNRAS, 424, 855

Kiewe M. et al., 2012, ApJ, 744, 10

Kochanek C. S., Szczygiel D. M., Stanek K. Z., 2011, ApJ, 737, 76

Lauberts A., Valentijn E. A., 1989, The Surface Photometry Catalogue of the ESO-Uppsala Galaxies. ESO, Garching

Levesque E. M., Stringfellow G. S., Ginsburg A. G., Bally J., Keeney B. A., 2012, preprint (arXiv:1211.4577)

Liu Q.-Z., Hu J.-Y., Hang H.-R., Qiu Y.-L., Zhu Z.-X., Qiao Q.-Y., 2000, A&AS, 144, 219

Maercker M. et al., 2012, Nat, 490, 232

Mauerhan J., Smith N., 2012, MNRAS, 424, 2659

Mauerhan J. C. et al., 2013a, MNRAS, 430, 1801

Mauerhan J. C. et al., 2013b, MNRAS, 431, 2599

Maund J. R. et al., 2006, MNRAS, 369, 390

Maza J. et al., 2009, Cent. Bur. Electron. Telegrams, 1928, 1

Milisavljevic D., Fesen R. A., Chevalier R. A., Kirshner R. P., Challis P., Turatto M., 2012, ApJ, 751, 25

Osterbrock D. E., Ferland G. J., 2006, Astrophysics of Gaseous Nebulae and Active Galactic Nuclei, 2nd edn. University Science Books, Sausalito, CA

Pastorello A. et al., 2007, Nat, 447, 829

Pastorello A. et al., 2008, MNRAS, 389, 131

Pastorello A. et al., 2010, ApJ, 408, 181

Pastorello A. et al., 2013, 767, 1 (P13)

Poole T. S. et al., 2008, MNRAS, 383, 627

Potashov M., Blinnikov S., Baklanov P., Dolgov A., 2013, MNRAS, 431, L98

Prieto J. L., Brimacombe J., Drake A. J., Howerton S., 2013, ApJ, 763, L27

Quataert E., Shiode J., 2012, MNRAS, 423, L92

Reichart D. et al., 2005, Nuovo Cimento C, 28, 767

Rybicki G. B., Lightman A. P., 1979, Radiative Processes in Astrophysics. Wiley-Interscience, New York, p. 393

Schlegel E. M., 1990, MNRAS, 244, 269

Smartt S. J., Eldridge J. J., Crockett R. M., Maund J. R., 2009, MNRAS, 395, 1409

Smith N. et al., 2007, ApJ, 666, 1116

Smith N. et al., 2010a, AJ, 139, 1451

Smith N., Chornock R., Silverman J. M., Filippenko A. V., Foley R. J., 2010b, ApJ, 709, 856

Smith N., Li W., Filippenko A. V., Chornock R., 2011a, MNRAS, 412, 1522

Smith N. et al., 2011b, ApJ, 732, 63

Sobolev V. V., 1960, Moving Envelopes of Stars. Harvard Univ. Press, Cambridge

Soker N., Kashi A., 2013, ApJ, 764, L6

Sollerman J., Cumming R. J., Lundqvist P., 1998, ApJ, 493, 933

Stritzinger M. et al., 2012, ApJ, 756, 173

Suntzeff N. B., Bouchet P., 1990, AJ, 99, 650

Trundle C., Kotak R., Vink J. S., Meikle W. P. S., 2008, A&A, 483, L47

Turatto M., Cappellaro E., Danziger I. J., Benetti S., Gouiffes C., della Valle M., 1993, MNRAS, 262, 128

Turatto M. et al., 1998, ApJ, 498, L129

Umeda H., Nomoto K., 2008, ApJ, 673, 1014

Van Dokkum P. G., 2001, PASP, 113, 1420

Van Dyk S. D., Matheson T., 2012, ApJ, 746, 179

Van Dyk S. D., Peng C. Y., King J. Y., Filippenko A. V., Treffers R. R., Li W., Richmond M. W., 2000, PASP, 112, 1532

Verner D. A., Ferland G. J., Korista K. T., Yakovlev D. G., 1996, ApJ, 465, 487

Weiler K. W., van Dyk S. D., Pringle J. E., Panagia N., 1992, ApJ, 399, 672

Weis K., Bomans D. J., 2005, A&A, 429, L13

Woosley S. E., Heger A., Weaver T. A., 2002, Rev. Mod. Phys., 74, 1015

Woosley S. E., Blinnikov S., Heger A., 2007, Nat, 450, 390

Yaron O., Gal-Yam A., 2012, PASP, 124, 668

Zhang T. et al., 2012, AJ, 144, 131

Zwicky F., 1964, ApJ, 139, 514

APPENDIX A: NLTE MODELLING FOR THE NARROW H LINES IN SN 2009IP

We compute NLTE solutions for the ionization and excitation balance of hydrogen, taking all radiative processes due to the photospheric radiation field into account, along with all bound–bound collisional transitions. We use a model atom including fine structure with $N = 210$ nl levels ($n = 1-20$), with energy levels and A-values from NIST, bound–bound collision rates from Johnson (1972) and Anderson et al. (2000), photoionization cross-sections from Verner et al. (1996) for $n = 1$ and scaled to $n \geq 2$ according to Rybicki & Lightman (1979), and radiative recombination rates from Brocklehurst (1971). We do not include collisional ionization or its inverse process three-body recombination, which start to become important only at high densities ($n \gtrsim 10^{13}$ cm^{-3}).

We take radiative transfer effects into account by using escape probabilities. In the limit of small velocity gradients (dV/d$r \ll \Delta V_{\mathrm{thermal}}/\Delta r$), we use the position-averaged escape probability in

a uniform sphere (Osterbrock & Ferland 2006)[10]

$$\beta(\tau_{ij}) = \frac{3}{4\tau_{ij}} \left[1 - \frac{1}{2\tau_{ij}^2} + \left(\frac{1}{\tau_{ij}} + \frac{1}{2\tau_{ij}^2} \right) e^{-2\tau_{ij}} \right] \quad (A1)$$

$$\tau_{ij} = \frac{A_{ij}\lambda_{ij}^3}{8\pi^{3/2}} \frac{g_j}{g_i} \left(n_i - n_j \frac{g_i}{g_j} \right) \left(\frac{\Delta V_{\text{thermal}}}{\Delta r} \right)^{-1}, \quad (A2)$$

where i and j refer to the levels (i is the lower one here), g_i and g_j are the statistical weights, A_{ij} is the Einstein coefficient for spontaneous decay, λ_{ij} is the line wavelength, $\Delta V_{\text{thermal}}$ is the thermal velocity dispersion

$$\Delta V_{\text{thermal}} = \sqrt{\frac{2kT}{m_p}} \quad (A3)$$

and Δr is the effective column length, given by

$$\Delta r = \frac{1}{n_i(R_{\text{in}}) - n_j(R_{\text{in}})\frac{g_i}{g_j}} \int_{R_{\text{in}}}^{R_{\text{ion}}} n_i(r) - n_j(r) \frac{g_i}{g_j} dr, \quad (A4)$$

where R_{ion} is the outer limit of the ionized region (computed iteratively).

In the limit of large velocity gradients ($dV/dr \gg \Delta V_{\text{thermal}}/\Delta r$), we instead use the Sobolev approximation (Sobolev 1960; Castor 1970)

$$\beta(\tau_{ij}^s) = \frac{1 - e^{-\tau_{ij}^s}}{\tau_{ij}^s} \quad (A5)$$

$$\tau_{ij}^s = \frac{A_{ij}\lambda_{ij}^3}{8\pi} \frac{g_j}{g_i} \left(n_i - n_j \frac{g_i}{g_j} \right) \left(\frac{dV(r)}{dr} \right)^{-1}. \quad (A6)$$

Since $\tau_{ij}^s/\tau_{ij} \approx \Delta V_{\text{thermal}}/\Delta V_{\text{flow}}$, where $\Delta V_{\text{flow}} \sim \frac{dV}{dr}\Delta r$, rapid flows ($\Delta V_{\text{flow}} > \Delta V_{\text{thermal}}$) have the effect of lowering the line optical depths, enhancing the escape probabilities.

A priori, the velocity gradients in the CSM of SN2009ip are unknown. The gradient could quite possibly be important, since typical expansion velocities of the narrow lines in the spectra are of the order of $\Delta V_{\text{flow}} \sim 10^3$ km s^{-1}, whereas the thermal velocities are of the order of $\Delta V_{\text{thermal}} \sim 10$ km s^{-1} (assuming $T \sim 10^4$ K). If the CSM was created by an eruption, the velocity field will be close to homology with a gradient of $\frac{dV}{dr} = t^{-1}$, where t is the time since the eruption. If the CSM instead originates in a steady wind, and accelerations in the wind are small, the gradient can be insignificant over the emission region.

We explore models with different assumptions about the velocity field. We introduce a default velocity gradient $\frac{dV}{dr0}$ by taking the ratio of the typical CSM velocity (10^3 km s^{-1}) to the system scale size (10^4 R$_\odot$), so

$$\frac{dV}{dr0} = 1.4 \times 10^{-7} \text{ s}^{-1}. \quad (A7)$$

---

[10] Various flavours of escape probabilities may be used depending on the assumed geometry and density profile of the emitting region as well as the details of the radiative transfer approximations (Capriotti 1965; Drake & Ulrich 1980; Osterbrock & Ferland 2006), but for our purposes trying to select the 'best' ones is not meaningful, as they only differ by a factor of a few at most. Note that we also use the escape probabilities at line centre, rather than the line-profiled average expression, as these generally differ by less than a factor of 2.

For an eruptive origin, this corresponds to $t = 80$ d. We later try models with $\frac{dV}{dr} = \epsilon \frac{dV}{dr0}$, for different values of ϵ.

A1 NLTE solutions

The bound–bound radiative rates due to the external radiation field are computed by (e.g. Castor 1970; Elitzur 1982)

$$R_{ij} = B_{ij} J_{\nu_{ij}} \beta(\tau_{ij}) \text{ s}^{-1}, \quad (A8)$$

where B_{ij} is the Einstein coefficient for photoabsorption ($i < j$) and stimulated emission ($i > j$), $J_{\nu_{ij}}$ is the mean intensity at the line frequency ν_{ij} (excluding any attenuation by the line) and $\beta(\tau_{ij})$ is the escape probability (described above). Close to the photosphere we have

$$J_\nu = \frac{1}{4\pi} \int_0^{2\pi} d\phi \int_0^{\pi/2} B_\nu \sin\theta \cos\theta d\theta = \frac{1}{4} B_\nu. \quad (A9)$$

The photoionization rate for level i is

$$\Gamma_i = \int_{\nu_0^i}^\infty \frac{4\pi J_\nu}{h\nu} \sigma_\nu^i d\nu \text{ s}^{-1}, \quad (A10)$$

where σ_ν^i is the ionization cross-section for level i and ν_0^i is the threshold frequency. The total photoionization rate is

$$\Gamma = \sum_{i=1}^N \Gamma_i \frac{n_i}{n_{\text{HI}}} \text{ s}^{-1}, \quad (A11)$$

where $n_{\text{HI}} = \sum_{i=1}^N n_i$ and n_i is the level population of level i (computed iteratively).

The ionization balance equation is, approximating the proton density to equal the electron density ($n_+ = n_e$),

$$\Gamma n(1 - x_e) = (\alpha + \alpha_{\text{stim}}) n^2 x_e^2, \quad (A12)$$

where x_e is the electron fraction ($= n_e/n$) and α is the effective (including optical depth effects) spontaneous radiative recombination coefficient

$$\alpha = \sum_{i=1}^N \alpha_i \beta(\tau_i), \quad (A13)$$

where $\beta(\tau_i)$ is computed with the static escape probability formalism (equation A1), and α_{stim} is the stimulated recombination coefficient

$$\alpha_{\text{stim}} = \sum_{i=1}^N \frac{g_i}{2} \left(\frac{2\pi m_e kT}{h^2} \right)^{-3/2} \int_{\nu_0^i}^\infty \frac{4\pi J_\nu}{h\nu} \sigma_\nu^i e^{-(h\nu - h\nu_0^i)/kT} d\nu. \quad (A14)$$

Equation (A12) is solved by the Newton–Raphson method.

For a given solution to x_e [and thereby for $n_+ = n_e = nx_e$ and $n_{\text{HI}} = n(1 - x_e)$], we then solve the set of statistical equilibrium equations for the excited levels of H I. For level i,

$$\left[\alpha_i \beta(\tau_i) + \alpha_{\text{stim}}^i \right] n_e^2 + \sum_{j \neq i} n_j \left[C_{ji} n_e + A_{ji} \beta_{ji} + R_{ji} \right] \quad (A15)$$

$$= n_i \left[\Gamma_i + \sum_{j \neq i} \left(A_{ij} \beta_{ij} + C_{ij} n_e + R_{ij} \right) \right], \quad (A16)$$

where α_i is the specific radiative recombination coefficient, C_{ij} are the bound–bound collision coefficients and the other symbols are defined above. Since the escape probabilities β_{ij} depend on the

level populations themselves, the system is non-linear and is solved iteratively.

Together with the number conservation equation (we ignore contributions by He and metals to n_e, since this contribution is small unless very high ionization states are reached for the metals)

$$n_{\rm HI} + n_e = n \qquad (A17)$$

we then iteratively solve for ionization balance, level populations and line optical depths, for given values of n and T_* (T is taken as $= T_*$). This allows us to compute line optical depths and emissivity ratios for models in the Sobolev limit, where these quantities only depend on local conditions

If we assume a density profile for the CSM, we can also compute solutions for steady flows ($\mathrm{d}V/\mathrm{d}r = 0$), as well as integrated quantities such as total line luminosities and continuum optical depths in all the models. The size of the ionized region can be estimated by equating the number of absorbed continuum photons to the number of recombinations

$$\sum_{i=1}^{N} \int_{\nu_0^i}^{\nu_0^{i-1}} \frac{4\pi J_\nu}{h\nu} \left[1 - e^{-\sum \tau_j(R_{\rm ion})} \right] \mathrm{d}\nu = \int_{R_{\rm in}}^{R_{\rm ion}} 4\pi r^2 n(r)^2 \alpha \, \mathrm{d}r \qquad (A18)$$

which can be solved for $R_{\rm ion}$ given a density profile $n(r)$. The continuum optical depths are computed by equation (A21).

For small enough densities, there is no solution as recombinations are too slow to bound an H II region, and the ionized region is then formally infinite (in actuality it is bounded by time travel limits, or when it encounters the interstellar medium).

Given the solution to $R_{\rm ion}$, the electron scattering optical depth is

$$\tau_{\rm es} = \sigma_{\rm es} \int_{R_{\rm in}}^{R_{\rm ion}} n_e(r) \, \mathrm{d}r, \qquad (A19)$$

which for $n_e(r) = n_e(R/R_{\rm in})^{-p}$ ($p \geq 2$) equals

$$\tau_{\rm es} = \sigma_{\rm es} n_e(R_{\rm in}) R_{\rm in} \frac{1 - \left(\frac{R_{\rm in}}{R_{\rm ion}} \right)^{p-1}}{p - 1}, \qquad (A20)$$

where $\sigma_{\rm es} = 6.65 \times 10^{-25} \, {\rm cm}^2 \, {\rm g}^{-1}$. For the level populations, it is a reasonable approximation that $n_i(r) \propto r^{2p}$, since recombination rates scale with $n_e^2 \approx n^2$ (through the dilution of the photospheric radiation field for photoexcitation and through the n_e^2 dependence for recombination). Thus, for the photoionization optical depths

$$\tau_i \approx \sigma_i(\nu_0^i) n_i(R_{\rm in}) R_{\rm in} \frac{1 - \left(\frac{R_{\rm in}}{R_{\rm ion}} \right)^{2p-1}}{2p - 1}. \qquad (A21)$$

To clarify, we thus compute the NLTE solutions explicitly for the density and radiation field specified at the inner region, and assume scalings of the solutions at larger radii according to $n_e \propto r^{-p}$ and $n_i \propto r^{-2p}$. In all the solutions presented in the paper, we use $p = 2$, corresponding to a steady mass-loss.

APPENDIX B: TABLES

Table B1. Optical photometry of SN 2009ip in the Landolt system; uncertainties are given in parentheses.

Date	MJD	U	B	V	R	I	Instrument
09-10-12	562 09.04	13.00 (0.04)	13.87 (0.02)	13.90 (0.01)	13.75 (0.01)	13.68 (0.01)	EFOSC2
10-10-12	562 10.27	13.04 (0.02)	13.93 (0.01)	13.93 (0.01)	13.78 (0.01)	13.69 (0.01)	EFOSC2
15-10-12	562 15.24	13.15 (0.02)	14.01 (0.01)	13.97 (0.01)	13.79 (0.01)	13.72 (0.01)	EFOSC2
16-10-12	562 16.02	13.22 (0.01)	14.09 (0.01)	14.06 (0.01)	13.87 (0.01)	13.79 (0.01)	EFOSC2
16-10-12	562 16.71	13.34 (0.05)	14.16 (0.05)	14.03 (0.05)	–	–	UVOT
16-10-12	562 16.77	–	14.28 (0.05)	–	–	–	UVOT
18-10-12	562 18.01	–	14.40 (0.02)	14.17 (0.02)	13.97 (0.02)	13.92 (0.04)	PROMPT
19-10-12	562 19.02	–	–	14.21 (0.01)	14.04 (0.03)	13.95 (0.03)	PROMPT
18-10-12	562 19.32	13.82 (0.05)	14.37 (0.05)	14.20 (0.05)	–	–	UVOT
20-10-12	562 20.89	13.84 (0.03)	14.45 (0.06)	14.28 (0.04)	14.09 (0.04)	13.99 (0.05)	RATCAM
20-10-12	562 20.96	13.88 (0.04)	–	–	–	–	UVOT
20-10-12	562 21.04	13.90 (0.05)	14.47 (0.05)	14.30 (0.05)	–	–	UVOT
20-10-12	562 21.18	13.80 (0.04)	14.51 (0.01)	14.34 (0.01)	14.15 (0.01)	14.02 (0.01)	EFOSC2
21-10-12	562 21.91	13.89 (0.02)	14.51 (0.02)	14.35 (0.01)	14.15 (0.01)	–	RATCAM
22-10-12	562 22.78	13.93 (0.05)	14.61 (0.05)	14.45 (0.05)	–	–	UVOT
22-10-12	562 22.92	14.07 (0.10)	14.68 (0.02)	14.41 (0.02)	14.19 (0.02)	14.15 (0.02)	RATCAM
23-10-12	562 23.07	–	–	14.40 (0.01)	14.22 (0.01)	14.15 (0.04)	PROMPT
23-10-12	562 23.25	14.13 (0.03)	14.59 (0.02)	14.44 (0.01)	14.24 (0.01)	14.12 (0.02)	EFOSC2
24-10-12	562 24.87	14.20 (0.02)	14.74 (0.01)	14.48 (0.02)	14.29 (0.01)	14.22 (0.05)	RATCAM
24-10-12	562 24.99	14.26 (0.06)	14.66 (0.03)	14.49 (0.06)	–	–	UVOT
25-10-12	562 25.02	–	14.79 (0.02)	14.54 (0.05)	14.29 (0.03)	14.22 (0.02)	PROMPT
24-10-12	562 25.12	14.27 (0.05)	–	–	–	–	UVOT
25-10-12	562 25.88	14.33 (0.09)	14.86 (0.02)	14.65 (0.01)	14.41 (0.01)	14.34 (0.03)	RATCAM
26-10-12	562 26.73	14.62 (0.06)	14.92 (0.05)	14.69 (0.06)	–	–	UVOT
28-10-12	562 28.86	14.97 (0.06)	–	–	–	–	UVOT
29-10-12	562 29.05	–	15.42 (0.05)	15.02 (0.03)	14.74 (0.04)	14.61 (0.04)	PROMPT
28-10-12	562 29.21	15.03 (0.06)	15.23 (0.06)	15.00 (0.07)	–	–	UVOT
30-10-12	562 30.87	15.38 (0.06)	15.57 (0.05)	15.13 (0.06)	–	–	UVOT
31-10-12	562 31.03	–	15.49 (0.03)	–	–	–	PROMPT
01-11-12	562 33.35	15.25 (0.06)	15.39 (0.06)	14.97 (0.06)	–	–	UVOT

Table B1 – *continued*

Date	MJD	U	B	V	R	I	Instrument
03-11-12	562 34.98	15.17 (0.05)	15.22 (0.05)	14.78 (0.06)	–	–	UVOT
05-11-12	562 36.09	14.87 (0.01)	15.21 (0.01)	14.92 (0.06)	14.71 (0.01)	14.36 (0.04)	EFOSC2
05-11-12	562 36.71	15.02 (0.05)	15.17 (0.06)	14.81 (0.05)	–	–	UVOT
06-11-12	562 37.07	–	15.32 (0.03)	–	–	–	PROMPT
07-11-12	562 38.03	–	15.37 (0.04)	15.07 (0.03)	14.84 (0.03)	14.68 (0.03)	PROMPT
07-11-12	562 38.55	15.39 (0.05)	15.40 (0.04)	15.15 (0.07)	–	–	UVOT
08-11-12	562 39.02	–	15.56 (0.02)	–	–	–	PROMPT
08-11-12	562 39.14	15.33 (0.01)	15.56 (0.01)	15.26 (0.01)	14.96 (0.02)	14.80 (0.02)	EFOSC2
09-11-12	562 40.55	15.68 (0.05)	15.74 (0.05)	15.29 (0.06)	–	–	UVOT
11-11-12	562 42.04	–	15.99 (0.05)	15.50 (0.02)	15.21 (0.02)	15.03 (0.04)	PROMPT
11-11-12	562 42.79	16.11 (0.07)	16.14 (0.06)	15.57 (0.06)	–	–	UVOT
11-11-12	562 42.80	16.08 (0.05)	16.09 (0.02)	15.60 (0.05)	15.26 (0.07)	15.03 (0.05)	RATCAM
12-11-12	562 43.04	–	16.13 (0.04)	15.59 (0.02)	15.24 (0.03)	15.11 (0.04)	PROMPT
13-11-12	562 44.04	–	16.17 (0.02)	15.67 (0.02)	15.35 (0.02)	15.15 (0.04)	PROMPT
13-11-12	562 44.92	16.39 (0.07)	16.24 (0.06)	15.71 (0.06)	–	–	UVOT
13-11-12	562 44.82	16.281 (0.09)	16.30 (0.06)	15.69 (0.02)	15.35 (0.08)	15.22 (0.03)	RATCAM
14-11-12	562 46.11	–	–	–	15.37 (0.02)	–	EFOSC2
15-11-12	562 46.17	–	16.29 (0.03)	15.70 (0.07)	15.42 (0.03)	15.22 (0.05)	PROMPT
15-11-12	562 47.41	16.52 (0.08)	16.41 (0.05)	15.81 (0.07)	–	–	UVOT
17-11-12	562 48.54	16.58 (0.06)	16.43 (0.06)	15.85 (0.07)	–	–	UVOT
18-11-12	562 49.08	–	16.43 (0.03)	15.80 (0.03)	15.48 (0.02)	15.27 (0.04)	PROMPT
19-11-12	562 50.54	16.87 (0.09)	16.59 (0.07)	15.96 (0.07)	–	–	UVOT
21-11-12	562 52.13	–	16.76 (0.03)	16.04 (0.06)	15.69 (0.04)	15.45 (0.06)	PROMPT
21-11-12	562 52.16	17.12 (0.02)	16.77 (0.01)	16.21 (0.06)	15.73 (0.04)	15.48 (0.02)	EFOSC2
21-11-12	562 53.08	17.15 (0.09)	16.82 (0.06)	16.15 (0.08)	–	–	UVOT
23-11-12	562 54.58	17.51 (0.09)	16.87 (0.07)	16.29 (0.07)	–	–	UVOT
25-11-12	562 56.14	–	16.95 (0.05)	16.25 (0.04)	15.81 (0.04)	15.52 (0.05)	PROMPT
25-11-12	562 57.17	17.64 (0.08)	17.04 (0.07)	16.38 (0.09)	–	–	UVOT
27-11-12	562 59.03	17.66 (0.08)	17.19 (0.08)	16.47 (0.07)	–	–	UVOT
29-11-12	562 60.83	17.64 (0.09)	17.19 (0.07)	16.52 (0.07)	–	–	UVOT
30-11-12	562 61.15	–	17.06 (0.04)	16.37 (0.03)	–	–	PROMPT
01-12-12	562 62.70	17.62 (0.08)	17.18 (0.07)	16.47 (0.07)	–	–	UVOT
03-12-12	562 64.08	–	17.22 (0.04)	16.40 (0.01)	15.93 (0.02)	15.62 (0.05)	PROMPT
03-12-12	562 64.82	17.46 (0.10)	17.14 (0.07)	16.48 (0.04)	15.86 (0.08)	15.70 (0.05)	RATCAM
03-12-12	562 65.06	17.66 (0.10)	17.31 (0.06)	16.54 (0.04)	16.06 (0.03)	15.66 (0.05)	EFOSC2
03-12-12	562 65.11	17.82 (0.09)	17.37 (0.08)	16.69 (0.07)	–	–	UVOT
05-12-12	562 66.65	18.01 (0.12)	17.68 (0.09)	16.72 (0.08)	–	–	UVOT
07-12-12	562 69.16	18.59 (0.17)	18.16 (0.11)	17.04 (0.11)	–	–	UVOT
09-12-12	562 70.85	18.87 (0.24)	18.31 (0.14)	17.32 (0.13)	–	–	UVOT
11-12-12	562 72.08	–	18.34 (0.04)	17.30 (0.04)	16.62 (0.03)	16.32 (0.09)	PROMPT
11-12-12	562 72.76	18.97 (0.21)	18.52 (0.14)	17.46 (0.14)	–	–	UVOT
11-12-12	562 73.05	–	–	–	16.72 (0.05)	–	EFOSC2
13-12-12	562 74.62	19.06 (0.42)	18.86 (0.33)	18.06 (0.30)	-	-	UVOT
14-12-12	562 75.07	–	19.03 (0.06)	18.00 (0.05)	17.22 (0.04)	16.94 (0.07)	PROMPT
15-12-12	562 76.73	–	19.30 (0.22)	18.53 (0.21)	–	–	UVOT
17-12-12	562 78.05	–	19.16 (0.10)	18.35 (0.14)	17.46 (0.11)	17.24 (0.11)	PROMPT
20-12-12	562 82.09	19.452 (0.10)	19.22 (0.09)	18.27 (0.06)	17.42 (0.05)	17.15 (0.10)	EFOSC2
29-12-12	562 90.07	–	>18.0	18.55 (0.11)	–	–	PROMPT

Table B2. UV photometry of SN 2009ip from *Swift*+UVOT, together with errors in parentheses. All values are in the UVOT system.

Date	MJD	$uvw2$	$uvm2$	$uvw1$
16-10-12	562 16.71	13.39 (0.05)	13.12 (0.05)	13.33 (0.05)
16-10-12	562 16.87	13.54 (0.05)	–	–
16-10-12	562 16.90	–	13.29 (0.06)	–
18-10-12	562 19.32	14.20 (0.05)	13.97 (0.06)	13.79 (0.06)
20-10-12	562 20.93	14.58 (0.05)	–	–
20-10-12	562 21.04	14.59 (0.06)	14.39 (0.06)	14.10 (0.06)
22-10-12	562 22.78	14.90 (0.06)	14.55 (0.06)	14.26 (0.06)
22-10-12	562 22.98	–	14.56 (0.07)	–
22-10-12	562 22.99	14.70 (0.05)	–	–
24-10-12	562 24.99	15.29 (0.07)	14.93 (0.06)	14.48 (0.06)
24-10-12	562 25.00	–	15.15 (0.07)	–
24-10-12	562 25.14	15.31 (0.06)	–	–
26-10-12	562 26.73	15.54 (0.07)	15.26 (0.07)	14.85 (0.06)
28-10-12	562 29.21	15.98 (0.08)	15.61 (0.07)	15.39 (0.07)
30-10-12	562 30.87	16.51 (0.09)	16.00 (0.05)	15.59 (0.07)
01-11-12	562 33.35	16.64 (0.08)	16.19 (0.07)	15.76 (0.07)
02-11-12	562 34.28	16.64 (0.08)	16.27 (0.04)	–
03-11-12	562 34.98	16.68 (0.08)	16.20 (0.06)	15.64 (0.06)
05-11-12	562 36.71	16.68 (0.07)	16.42 (0.06)	15.65 (0.06)
07-11-12	562 38.55	16.51 (0.09)	16.20 (0.07)	15.58 (0.08)
09-11-12	562 40.55	17.19 (0.06)	16.74 (0.06)	16.06 (0.08)
11-11-12	562 42.79	17.57 (0.10)	16.91 (0.09)	16.45 (0.08)
13-11-12	562 44.92	17.81 (0.10)	17.51 (0.10)	17.08 (0.16)
15-11-12	562 47.41	18.00 (0.15)	17.70 (0.13)	17.26 (0.10)
17-11-12	562 48.54	18.15 (0.12)	17.80 (0.11)	17.28 (0.10)
19-11-12	562 50.54	18.43 (0.11)	17.98 (0.12)	17.35 (0.12)
21-11-12	562 53.08	18.94 (0.17)	18.68 (0.15)	17.57 (0.11)
23-11-12	562 54.58	19.19 (0.16)	18.75 (0.10)	17.75 (0.11)
25-11-12	562 57.17	19.45 (0.22)	19.06 (0.17)	18.07 (0.10)
27-11-12	562 59.03	19.68 (0.22)	19.26 (0.18)	18.22 (0.11)
29-11-12	562 60.83	20.08 (0.26)	19.14 (0.13)	18.36 (0.11)
01-12-12	562 62.70	20.10 (0.26)	19.59 (0.17)	18.72 (0.13)
03-12-12	562 65.11	20.10 (0.26)	19.56 (0.20)	18.68 (0.14)

Table B3. NIR photometry of SN 2009ip in the 2MASS system. Errors are given in parentheses.

Date	MJD	J	H	K	Instrument
12-10-12	56212.24	13.98 (0.07)	13.78 (0.04)	–	REMIR
19-10-12	56330.16	–	13.49 (0.07)	–	LUCIFER
20-10-12	56220.83	13.99 (0.08)	13.67 (0.04)	13.27 (0.08)	NOTCAM
21-10-12	56221.02	14.19 (0.13)	–	–	REMIR
22-10-12	56223.19	14.17 (0.02)	13.71 (0.04)	13.66 (0.13)	SOFI
26-10-12	56226.06	14.40 (0.12)	–	–	REMIR
05-11-12	56237.05	14.41 (0.08)	14.22 (0.11)	13.94 (0.12)	SOFI
11-11-12	56242.18	15.18 (0.08)	14.97 (0.10)	–	REMIR
13-11-12	56245.06	14.95 (0.07)	14.75 (0.08)	14.57 (0.06)	SOFI
04-12-12	56266.02	15.33 (0.04)	15.09 (0.08)	14.91 (0.05)	SOFI
21-12-12	56283.08	16.88 (0.11)	16.62 (0.08)	16.29 (0.09)	SOFI

This paper has been typeset from a TEX/LATEX file prepared by the author.